Lehrstuhl für
Technische Dynamik
Prof. Dr.-Ing. habil. Sigrid Leyendecker

Report
Chair of Applied Dynamics
2019

FRIEDRICH-ALEXANDER
UNIVERSITÄT
ERLANGEN-NÜRNBERG
TECHNISCHE FAKULTÄT

Prof. Dr.-Ing. habil. S. Leyendecker
Lehrstuhl für Technische Dynamik
Friedrich-Alexander-Universität Erlangen-Nürnberg
Immerwahrstrasse 1
91058 Erlangen
Tel.: 09131 8561000
Fax.: 09131 8561011
www: http://www.ltd.tf.uni-erlangen.de

Editor: E. Fleischmann, D. Phansalkar

Contents

1 Preface

The present report compiles and reviews the research and teaching activities of the Chair of Applied Dynamics (LTD) at the Friedrich-Alexander-Universität Erlangen-Nürnberg from January to December 2019. On the research front, the Chair of Applied Dynamics focuses on multibody dynamics and robotics, motion capturing, biomechanics, structure preserving simulation and optimal control. The focus is primarily on methodological development of mathematical models and numerical approaches for dynamic and optimal control simulations. Such approaches can provide new insights into complex behavior e.g. biomechanical and biological systems.
The specific problems under investigation are related to modern life science and engineering application. For example, the multibody dynamics of human motion (human grasping, gait cycle), robot motion (industrial, spatial and medical), the electro-mechanical modeling and simulation of muscles (heart project, muscle wrapping, artificial muscles), modeling and simulation of dynamic fracture and as well as the characterisation of bio-macromolecules.
The heart project includes the finite element modeling of the electrophysiological and mechanical processes and their coupling. With the advanced motion capturing laboratory at LTD, research encompasses experimental parameter identification, modeling, and simulation of these dynamical systems and in particular their optimal control. At the atomistic level, kinematic and geometric models are developed to obtain insights into macromolecules and their molecular mechanisms. To bridge the different scales that occur within and across these projects, accurate and efficient simulation techniques are of the essence. Thus, further projects are especially concerned with the development of (variational) integrator for systems with multiscale and multirate dynamics, higher order variational integrators, or Lie group methods, e.g., for use in geometrically exact beam dynamics or also to investigate kinetics in fracture mechanics with the help of structure preserving integrators.
The development of numerical methods is likewise important as the modelling of the nonlinear systems, whereby the formulation of variational principles plays a significant role on the levels of dynamic modeling, optimal control as well as numerical approximation.

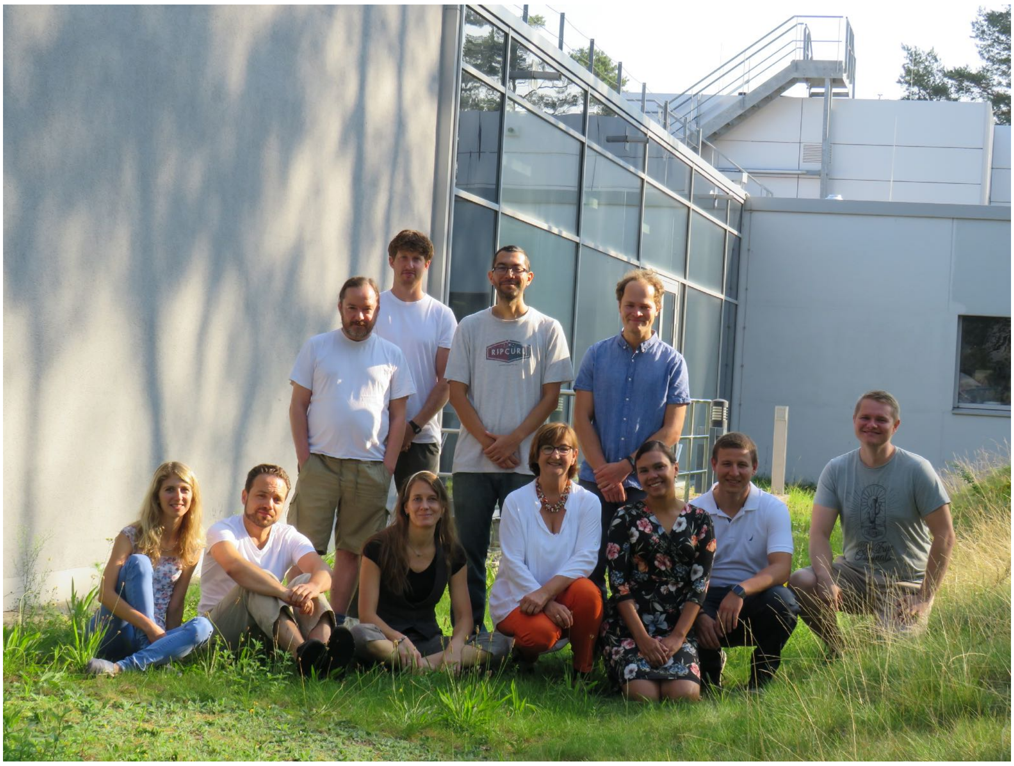

2 Team

chair holder
Prof. Dr.-Ing. habil. Sigrid Leyendecker

technical staff

Beate Hegen	
Elisa Fleischmann	from 15.05.2019
Sven Lässig	
Johannes Rössler	until 31.03.2019

academic scientist
Dr. rer. nat. Holger Lang

postdoc

Dr. Rodrigo Sato Martín de Almagro	from 15.08.2019

scientific staff

M.Sc.hons. Xiyu Chen	from 01.06.2019
M.Sc. David Holz	
M.Sc. Michael Klebl	from 01.07.2019
M.Sc. Denisa Martonová	from 01.02.2019
M.Sc. Johann Penner	
M.Sc. Dhananjay Phansalkar	from 01.05.2019
M.Sc. Uday Phutane	
M.Sc. Eduard Sebastian Scheiterer	from 01.05.2019
M.Sc. Theresa Wenger	

students

Yusuv Atakan	Niko Beck	Anja Boebel
Marc Milene Boum	Dorothea Brackenhammer	Katharina Fiedler
Ameni Gatri	Natalja Haigis	Simon Heinrich
Martin Hoffmann	Daphne Hohbohm	Xuyue Huang
Thomas Hufnagel	Simon Kaup	Abdul Waseh Khawaja
Lea Köstler	Marie Laurien	Teke Linonge
Markus Lohmayer	Nils Mößner	Tanya Neeraj
Carmen Neubauer	Arlette Ngnogue Kaptouom	Sebastian Penzl
Vijayan Prabhu	Matthias Pschorr	Sebastian Scheiterer
Syrine Slim	Bastian Stahl	Linghui Wang
Felix Werner	Simon Wiesheier	Fabian Wonn
Annalena Wrobel	Cikai Yu	Yusuv Zou

Student assistants are mainly active as tutors for young students in basic and advanced lectures at the Bachelor and Master level. Their contribution to high quality teaching is indispensable, thus financial support from various funding sources is gratefully acknowledged.


B. Hegen


E. Fleischmann


S. Lässig


J. Rößler


H. Lang

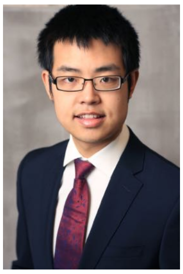
X. Chen


D. Holz


M. Klebl


D. Martonová

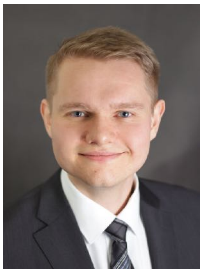
J. Penner


D. Phansalkar


U. Phutane


R. Sato


E.S. Scheiterer


T. Wenger


S. Leyendecker

3 Research

3.1 ETN – THREAD

The new ETN (European Training Network) project "Joint Training on Numerical Modelling of Highly Flexible Structures for Industrial Applications – THREAD" funded by the European Commission's Marie Skłodowska Curie Programme which is part of Horizon 2020. It will be coordinated by Prof. Dr. Martin Arnold from the Institute of Mathematics at the Martin Luther University Halle-Wittenberg (MLU). THREAD addresses the mechanical modelling, mathematical formulations and numerical methods for highly flexible slender structures like yarns, cables, hoses or ropes that are essential parts of high-performance engineering systems. The complex response of such structures in real operational conditions is far beyond the capabilities of current virtual prototyping tools. With 14 new PhD positions at 12 universitues and research institutions in Austria, Belgium, Croatia, France, Germany, Norway, Slovenia and Spain, the project brings mechanical engineers and mathematicians together around major challenges in industrial applications and open-source simulation software development. It stablishes an innovative modelling chain starting from detailed 3D modelling and experimental work to build validated 1D nonlinear rod models, which are then bought to a system-level simulation thanks to the outstanding numerical properties of the developed algorithms. This holistic approach combines advanced concepts in experimental and theoretical structural mechanics, non-smooth dynamics, computational geometry, discretisation methods and geometric numerical integration and will enable the next generation of virtual prototyping.

3.2 Heart project

The heart project is focusing on the modeling of the cardiac function to better understand cardiovascular disease, to be able to early detect or even predict heart failure and develop adequate patient specific therapies and medical devices. We are currently working on a rat as well as a human heart model. The former is related to the rat heart project, which is an established research cooperation between the Chair of Applied Dynamics and the Pediatric Cardiology at Friedrich-Alexander-Universität Erlangen-Nürnberg and is funded by the Klaus Tschira Stiftung. The goal of the project is to explore the heart function under pathological and normal conditions by developing a computational model of a rat heart which will be validated with experiments at the Pediatric Cardiology. Denisa Martonová, who joined the team in February, is working on the identification of the passive material parameters based on the experimental data from the Pediatric Cardiology. David Holz is mainly working on the transfer from the rat to the human heart model and is especially interested in the in vivo estimation of mechanical and electrophysiological properties. In 2019, we were mainly focusing on the transfer of the rat heart model to the human heart model, investigating the mechanoelectrical feedback in the currently used model as well as the modeling of the nonlinear fibre distribution in the myocardium. In the next step, the cardiac motion and hemodynamic response of the human heart model will be compared with MRI data provided by the Pediatric Cardiology.

3.3 FRASCAL – Fracture across Scales

The DFG research training group (RTG) FRASCAL - Fracture across Scales (GRK 2423) began at the start of this year (2019) with Prof. Dr.-Ing. habil. Paul Steinmann from the Chair of Applied Mechanics as spokesperson and is managed by the Central Institute for Scientific Computing (ZISC) of the Friedrich-Alexander-Universität Erlangen-Nürnberg. It encompass research groups from different departments of the Faculty of Sciences and the Faculty of Engineering. There are 12 project that are part of this RTG, with the project P9 – Adaptivity in the Dynamic Simulation of Fracture Mechanics is carried out by Dhananjay Phansalkar at LTD. This project aims to develop robust and efficient numerical techniques to investigate kinetics of fracture mechanics. It will require adaptive strategies to obtain suitable combinations of spatial and temporal mesh. These methods are developed in close cooperation with RTG's Mercator fellow Prof. Dr. Michael Ortiz.

3.4 Characterisation of Macromolecules

The characterisation of macromolecules project is a cooperation research between the Chair of Applied Dynamics at Friedrich-Alexander-Universität Erlangen-Nürnberg and SLAC National Accelerator Laboratory at Stanford University and is funded by German Research Foundation (DFG). The purpose of this project is characterizing macromolecules e.g. kinases by using the kino-geometric sampling (KGS) method. The rigidity and conformation transition analysis of macromolecules, will benefit drug development in the cancer field. The project is cooperated by Dr. Henry van den Bedem from Stanford University. Xiyu Chen, who joined the LTD team in June, is focusing on the rigidity analysis and the difference of activation states of kinases by using the KGS method.

3.5 BMBF 05M2016 – DYMARA

The DYMARA project is funded by the Federal Ministry of Education and Research (BMBF) under the funding priority "Healthy Life". The joint project is coordinated by Prof. Dr. rer. nat. habil. Bernd Simeon from Technische Universität Kaiserslautern (UNIKL) and has a thematic relation to ergonomics and health promotion at work. The aim of the project is to develop an innovative digital human model with detailed skeletal muscle modelling and fast numerical algorithms for fundamental research. As part of the collaborative project, Johann Penner at LTD investigates muscle paths in the biomechanical simulation of human motion and the integration of new fiber-based muscle models to multibody dynamics while the UNIKL is developing a continuum mechanical muscle model. The project partner Dr. Michael Burger from the Fraunhofer-Institut für Techno- und Wirtschaftsmathematik (ITWM) is focusing on the optimal control of the complete digital human model. Industrial partners are MaRhyThe-Systems GmbH & Co. KG. and flexStructures GmbH.

3.6 SPP 1886

The German Research Foundation (DFG) Priority Programme "Polymorphic uncertainty modelling for the numerical design of structures – SPP 1886" coordinated by Professor Dr.-Ing. Michael Kaliske from Technische Universität Dresden concluded its first phase with the annual meeting in Hamburg this year. Prof. Dr.-Ing. habil. Sigrid Leyendecker is part of the programme committee and principal investigator of one of the projects.

3.7 Scientific reports

The subsequent pages present a brief overview on the current research projects pursued at the Chair of Applied Dynamics. These are partly financed by third-party funding German Research Foundation (DFG), the Klaus Tschira Stiftung, the Federal Ministry of Education and Research (BMBF) and in addition by the core support of the university.

Research topics

Rigidity analysis with kino-geometric modeling of active and inactive kinases
Xiyu Chen, Sigrid Leyendecker, Henry van den Bedem

About the mechano-electrical feedback and the fibre orientation in cardiac modelling
David Holz, Minh Tuan Duong, Denisa Martonová, Muhannad Alkassar, Sven Dittrich, Sigrid Leyendecker

Optimisation simulations for kinematic parameter identification
Michael Klebl, Sigrid Leyendecker

Discrete Cosserat rods
Holger Lang, Sigrid Leyendecker, Joachim Linn

Characterisation of passive mechanical properties of healthy and infarcted rat myocardium
Denisa Martonová, Julia Seufert, David Holz, Minh Tuan Duong, Muhannad Alkassar and Sigrid Leyendecker

Biomechanical simulations with dynamic muscle paths on NURBS surfaces
Johann Penner, Sigrid Leyendecker

Challenges associated with quasi-static phase-field model for brittle fracture
Dhananjay Phansalkar, Sigrid Leyendecker

Optimal control grasping simulations for objective specific contact points
Uday Phutane, Michael Roller, Sigrid Leyendecker

High order variational integrators in constrained mechanical problems and field theories
Rodrigo T. Sato Martín de Almagro, Sigrid Leyendecker

A predeformed geometrically exact beam model for a dynamic-response prosthesis
Eduard S. Scheiterer, Sigrid Leyendecker

Rigidity analysis with kino-geometric modeling of active and inactive kinases

Xiyu Chen, Sigrid Leyendecker, Henry van den Bedem[1] [2]

Protein kinases are cellular enzymes which catalyse the phosphorylation reaction and they are also an important subject for drug research in cancer. Inhibitors are directed to its active or several inactive conformations, so the activation classification and the rigidity analysis of kinases may benefit drug development and general understanding of their conformation. V. Modia et al. [1] defined a new nomenclature for kinases and classified them into eight group clusters according to backbone conformations and orientation of phenylalanine.
For our numerical study, kino-geometric sampling (KGS) is an efficient method and a modeling framework to perform functional molecular rigidity analysis and to study transitions i.e. between active and inactive states. KGS represents molecules as articulated multi-body complexes with dihedral angles as revolute degrees of freedom and selected non-covalent interactions such as hydrogen bonds and hydrophobic interaction as holonomic constraints. Each hydrogen bonds interaction gives five constraints and only allows the hydrogen bond to rotate about the axis of the hydrogen bond, the constraint Jacobian matrix is given by derivation of the $5m$ hydrogen bond constraints with respect to d dihedral angle. Its sigular value decomposition (SVD) $\mathbf{JV} = \mathbf{U\Sigma}$ gives us two subspaces $\mathbf{U} = [u_1, ..., u_{5m}] \in R^{5m\times 5m}$ and $\mathbf{V} = [v_1, ..., v_d] \in R^{d\times d}$. The matrix $\mathbf{\Sigma} = diag(\sigma_1, ..., \sigma_p)$ where $p = min(5m, d)$ contains the singular value σ_i where $\sigma_1 \geq ... \geq \sigma_r \geq \sigma_{r+1} = ... = \sigma_p = 0$, the corresponding u_i and v_i are termed the i^{th} left and right singular vectors, respectively [2, 3]. Then, it can be seen that

$$\begin{aligned} range(\mathbf{J}) &= span\{u_1, ..., u_r\} \\ null(\mathbf{J}) &= span\{v_{r+1}, ..., v_d\} \end{aligned} \tag{1}$$

The nullspace of the Jacobian matrix defines the addmissible velocity for the dihedral angle and it also gives us information about rigidified dihedral angles and rigidified clusters. The rigidity of kinases is analyzed based on this information.
We based our work in the study of V. Modia et al. [1] and classified a large dataset of kinases in the protein data bank into different cluster groups according to structure similarity. 79 pdbfiles are selected based on structure similarity with the pdbfile 5UG9, which belongs to the inactive state group cluster DFGout_BBAminus and it is selected to compare with other group clusters. The active states and number of these kinases is shown in Table 1.

Group	DFGin	DFGin	DFGin	DFGin	DFGout
Cluster	BLAminus	ABAminus	BLBplus	BLBtrans	BBAminus
Active States	active	active	DFGup	DFGin-Trans	DFGout
Number	49	5	10	8	7

Table 1: 79 pdbfiles in this data subset

This subset contains 5 group clusters, the DFGin_BLAminus and DFGin_ABAminus are in the active states. Fig. 1A(left) shows the ratio of rigidified degrees of freedom (DoFs) to cycle degrees of freedom. For the active-state kinases, the ratio is larger for the inactive-state kinases with all the constraints, which means the active-state kinases in the subset are more rigid. In order to study the influence of the activation loop, Fig. 1A(right) shows the ratio of rigidified DoFs to cycle DoFs without constraints around the activation loop, the ratio is reduced for kinases in the active state, but the effect is not

[1]Atomwise, Inc. 717 Market Street, San Francisco, CA 94103 USA
[2]Department of Bioengineering and Therapeutic Sciences, UCSF, California, USA

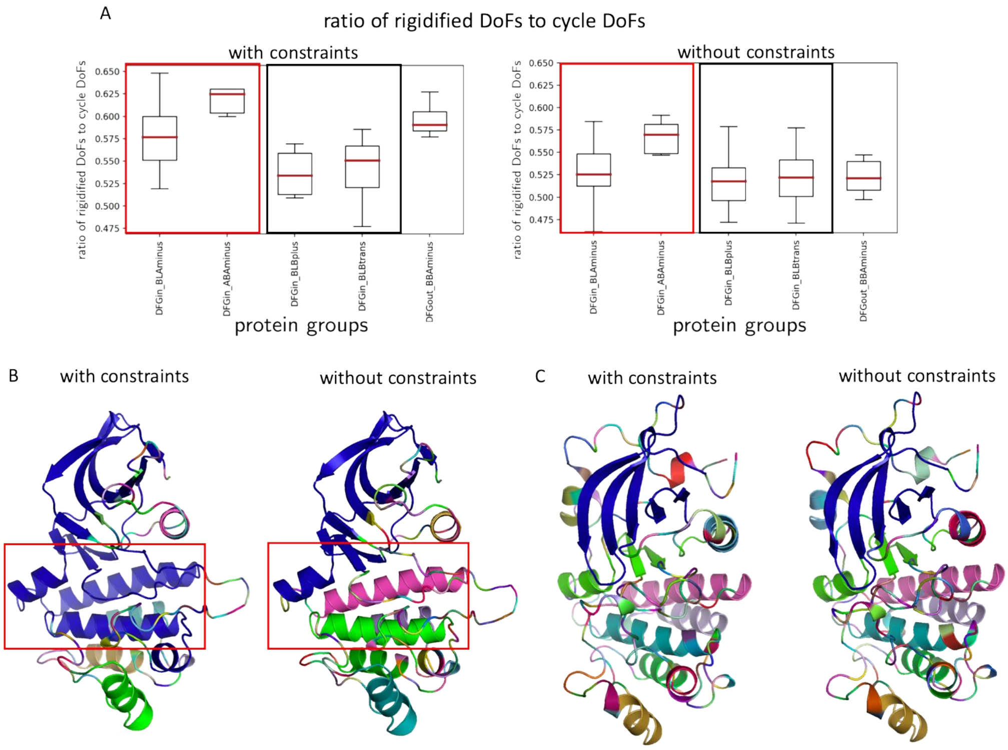

Figure 1: Influence of the activation loop of kinases for the data subset (A): Comparison of ratio of rigidified degrees of freedom to cycle degrees of freedom with and without the constraint around the activation loop. (B): visualisation of molecules of the active-state kinases (PDB:1U46 A) with and without constraint around the activation loop. (C): visualisation of molecules of the inactive-state kinases (PDB:3W2S A) with and without constraint around the activation loop

obvious for inactive-state kinases. Molecular visualisations are shown in order to compare the effect of enforcing the constraint around the activation loop in the case of active (Fig. 1B) and inactive-state kinases (Fig. 1C). The activation loop rigidifies the surrounding α-helix for the active-state kinases, but the difference is smaller for the inactive-state kinases. Overall, through the KGS rigidity analysis, differences in the ratio of rigidified DoFs to cycle DoFs between the active and the inactive state kinases are investigated. The results seem to indicate that the activation loop causes the active kinases to increase their rigidity, while it has less influence for the inactive kinases.

References

[1] M. Vivek, L. Roland, and J. Dunbrack. Defining a new nomenclature for the structures of active and inactive kinases. *PNAS*, **116**:6818-6827, 2019

[2] D. Budday, S. Leyendecker, and H. van den Bedem. Kinematic Flexibility Analysis: Hydrogen Bonding Patterns Impart a Spatial Hierarchy of Protein Motion. *Journal of Chemical Information and Modeling*, **58**(10):2108-2122, 2018

[3] D. Budday, S. Leyendecker, and H. van den Bedem. Geometric analysis characterizes molecular rigidity in generic and non-generic protein configurations. *Journal of the Mechanics and Physics of Solids*, **83**:36-47, 2015.

About the mechano-electrical feedback and the fibre orientation in cardiac modelling

David Holz, Minh Tuan Duong, Denisa Martonová, Muhannad Alkassar[1], Sven Dittrich[1], Sigrid Leyendecker

Nowadays, to fully understand the functionality of the cardiovascular system, computational models (often finite element models) are widely used. Two essential components of the finite element model of the heart are the mechano-electrical feedback (MEF) as well as the fibre orientation.
Here, we are investigating the interaction between different passive material models and the mechano-electrical feedback in cardiac modeling. Various types of passive mechanical laws (nearly incompressible/compressible, polynomial/exponential-type, transversally isotropic/orthotropic material models) are integrated in a fully coupled electromechanical model in order to study their specific interaction with the overall MEF behaviour [2].

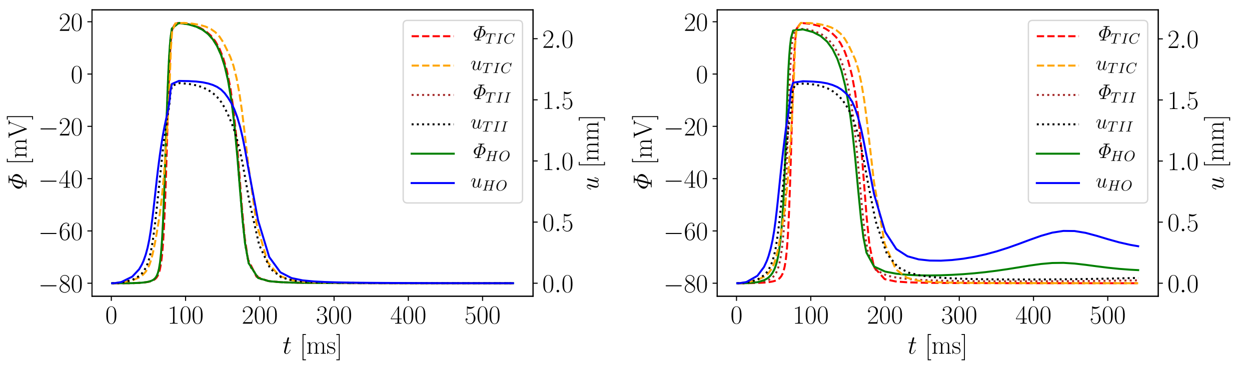

Figure 1: Evolution of AP Φ and displacement u of an apical node in a rat left ventricle for three models, without MEF (left) and with MEF using $G_s = 10$ (right).

The interaction between the passive models and the MEF is discussed through a computational study of a rat LV, whereby the following findings are obtained: i) compressibility: the transversely isotropic material law (TIC) predicts a significantly smaller fibre stretch (compression almost everywhere in the LV) and thus leads to a nearly unrecognisable change in the overall MEF behaviour (change in electrophysiology and mechanical contraction); additionally, for the incompressible models, we observe a residual deformation caused by a non-relaxed equilibrium, ii) polynomial vs. exponential material laws: due to the exponential strain energy function, the Holzapfel-Ogden (HO) model shows a faster temporal change of the fibre stretch in the depolarisation phase (leading to a faster depolarisation compared to the transversely isotropic incompressible material law (TII) model; higher MEF current) and at the same time slower temporal change of the fibre stretch in the late repolarisation phase, iii) transversely isotropic vs. orthotropic: the incompressibility condition with the associated stretches along the sheet and sheet normal direction on the boundaries, fibre stretch $\lambda < 1$ and thus the compression in fibre direction has to be compensated by stretch in the sheet and sheet normal direction) leads to a stretch in fibre direction in the middle layers. As the fibre stretch λ depends on the material properties in the sheet and sheet normal direction, there also exists a difference in the electromechanical behaviour and the MEF between a transversely isotropic and an orthotropic material law concerning the MEF behaviour.
Obviously, the type of passive material model plays a key role in defining the MEF behaviour in a fully coupled electromechanical model. It has to be further investigated which of the considered models reflect the cardiac tissue best concerning the overall MEF behaviour.

[1]Pediatric Cardiology, University of Erlangen Nuremberg, Loschgestrasse 15, 91054 Erlangen, Germany

The correct representation of the anatomy, or more specifically the fibre orientation, is another important ingredient in order to represent the electrical as well as the mechanical functionality in an appropriate way. The fibre orientation of the cardiac tissue can be measured e.g. using DT-MRI or histology. However, in the case that no patient-specific fibre orientation is known or only sparse data from clinical measurements is available, rule-based models are applied. Under these circumstances, it is assumed that the fibre angles are measured at discrete points of the heart, often on the endo- and epicardium (e.g. from simplified reference measurements on the surface rather than in the volume or layers). Additional information about the transmural change in fibre angle are obtained e.g. from histology slides. Here, however, we assume that a nonlinear function representing the transmural change in fibre angle is given, see Figure 2.

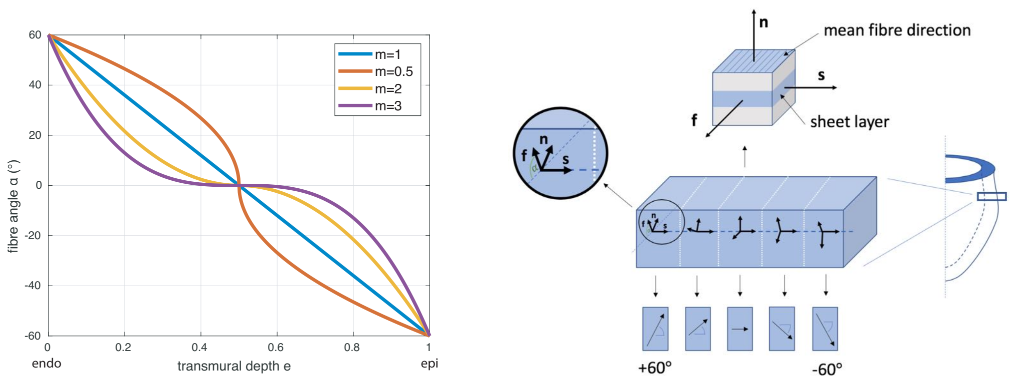

Figure 2: Left: transmural fibre angle $\alpha(e) = R * sgn(1-2e)|1-2e|^m$ depending on the transmural depth $e \in [0, 1]$, R =60° represents the maximum fibre angle, $m \in \mathbb{N}$ is to be chosen in accordance with clinical measurements, see [1]. Right: characteristic morphology of the cardiac tissue with the transmurally varying fibre direction $\boldsymbol{f}$, sheet direction $\boldsymbol{s}$ and normal direction $\boldsymbol{n}$.

We propose a method based on the reliable assessment of the ventricular myocardial thickness (transmural depth e) by solving both the Laplace equation and two first order partial differential equations, based on the approach by [3].

References

[1] V. Carapella, R. Bordas, P. Pathmanathan, M. Lohezic, J. Schneider, P. Kohl, K. Burrage and V. Grau. *Quantitative Study of the Effect of Tissue Microstructure on Contraction in a Computational Model of Rat Left Ventricle.* PLOS ONE **9:4**, 1–12 (2014).

[2] M. T. Duong, D. Holz, D. Martonová, K. Myoungsic, S. Dittrich, M. Alkassar and S. Leyendecker. *Interaction of the Mechano-Electrical Feedback With Passive Mechanical Models on a 3D Rat Left Ventricle: A Computational Study.* Front Physiol. **10**, 1041 (2019).

[3] S. E. Jones, B. R. Buchbinder, I. Aharon. *Three–dimensional mapping of cortical thickness using Laplace's equation.* Human brain mapping **11:1**, 12–32 (2000).

Optimisation simulations for kinematic parameter identification

Michael Klebl, Uday Phutane, Sigrid Leyendecker

Introduction In order to analyze biomechanical motions performed by humans, virtual human simulation is important for a wide range of applications like ergonomics, sports and healthcare. There is also great interest from the manufacturing industry for the purpose of ergonomic assessment and controlling assembly by humans. Simulation of human motion requires modeling in consideration of anthropometric variance. The foundation for modeling is a concept for parameter identification.

Motion capturing There are several techniques for motion capturing, such as X-rays, cinematography, etc. Compared to other motion capturing techniques, the marker based optical tracking system has the advantage to present the data in an absolute spatial reference system [5]. Optical capture systems based on retroreflective markers use high-resolution and high-speed infrared cameras, which are synchronised and calibrated. The marker positions are tracked by multiple cameras and their trajectories are estimated in 3D space by the optical motion capture system from the Qualisys tracking manager.

Kinematic Parameters As described in [1] the formulation of rigid bodies as discrete mechanical system subject to constraints is used for the multibody system. The configuration of each rigid body is described in director formulation, where generally the center of mass $\boldsymbol{\varphi} \in \mathbb{R}^3$ is relative to an orthonormal basis $\boldsymbol{e}_I$ fixed in space and an orthonormal body frame called directors $\boldsymbol{d}_1, \boldsymbol{d}_2, \boldsymbol{d}_3 \in \mathbb{R}^3$ is fixed at $\boldsymbol{\varphi}$. The time dependent configuration vector is given by $\boldsymbol{q}(t) = [\boldsymbol{\varphi}(t)\, \boldsymbol{d}_1(t)\, \boldsymbol{d}_2(t)\, \boldsymbol{d}_3(t)]^{\mathrm{T}} \in \mathbb{R}^{12}$. A material point $\boldsymbol{\rho} \in \mathbb{R}^3$ in the body's configuration is described as $\boldsymbol{\rho}(t) = \rho_I \boldsymbol{d}_I(t)$.
In the following two kinds of joints with two relative rotational degrees of freedom each are described. A common example for that within biomechanics is the elbow with flexion/extension and pronation/supination motion. The first kind is the cardan joint which is explained in [3]. It has two axes of rotation $\boldsymbol{n}^1$ and $\boldsymbol{n}^2$, that are intersecting and orthogonal to each other, $\boldsymbol{n}^1$ is fixed to the first body and $\boldsymbol{n}^2$ is fixed to the second body, $\boldsymbol{n}^1 = n^1{}_I \boldsymbol{d}_I^1$ and $\boldsymbol{n}^2 = n^2{}_I \boldsymbol{d}_I^2$. It is a special case of the second kind of joint, which is a non-intersecting and non-orthogonal (nino) joint as shown in [3]. A vector $\boldsymbol{d} = \boldsymbol{\varphi}^2 - \boldsymbol{\varphi}^1 + \boldsymbol{\rho}^2 - \boldsymbol{\rho}^1$ joins the points which define the locations for axes $\boldsymbol{n}^1$ and $\boldsymbol{n}^2$, respectively. Modifying the relations from [3] with the first body fixed in space will reduce the problem size. The kinematic update for the nino joint, through an increment $\boldsymbol{u}_{n+1} = \left(\theta^1_{n+1},\ \theta^2_{n+1}\right) \in \mathbb{R}^2$, where θ^1_{n+1} and θ^2_{n+1} are the incremental rotations around axes $\boldsymbol{n}^1$ and $\boldsymbol{n}^2$, respectively, is given for the configuration of the moving body as $\boldsymbol{\varphi}^2_{n+1} = \boldsymbol{\varphi}^2_n + \boldsymbol{\rho}^1_n + \exp\left(\widehat{\theta^1_{n+1}\boldsymbol{n}^1_n}\right) \cdot \boldsymbol{d}_n - \exp\left(\widehat{\theta^1_{n+1}\boldsymbol{n}^1_n}\right) \cdot \exp\left(\widehat{\theta^2_{n+1}\boldsymbol{n}^2_n}\right) \cdot \boldsymbol{\rho}^2_n$.

Example As an example a wood model is described as a multibody system consisting of two rigid bodies, see Figure 1. The rotation axes and the optical marker positions relative to the segments are computed from the measurement date via a non-linear kinematics optimisation. Thus, the exact definition of the created model is already a result from the measured data $\left\{\overline{\boldsymbol{m}}^\alpha_\beta|_n\right\}_{n=1}^N$ for marker $\beta = 1,2,3$ and for the body $\alpha = 1,2$. The optical measurements were collected from a Qualisys tracking system with ten Oqus cameras. For tracking the model, eleven retroreflective markers were used, four markers are on the fixed part, three markers on the moving part and two markers are placed on each axis line to estimate the rotation axes for initial configuration setup and error checking. A sequence of 10s with 100 Hz frame-rate was used. Within this sequence, a rotation was performed with respect to both axes for the moving body. A low pass butterworth filter with a cutoff frequency of 20 Hz is used for the measured data, the center position and directors for both bodies are obtained from the marker positions.

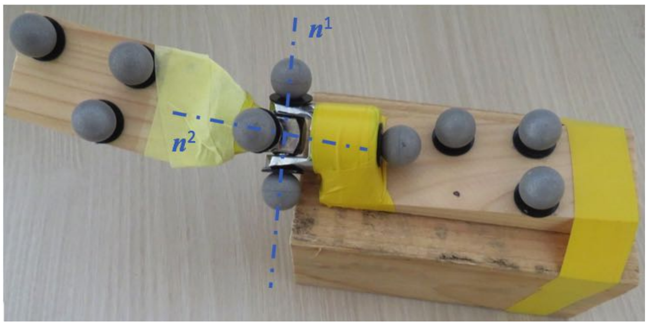

Figure 1: Wood model with optical markers and two rotaion axes

The nonlinear optimisation problem is solved in Matlab using fmincon with gradients computed using the automatic differentiation software framework CasADi [4]. The wood object with a two degree of freedom joint is modeled both as a cardan joint and as a nino joint. The unknown parameters $\boldsymbol{\rho}^\alpha$ and $\boldsymbol{n}^\alpha$ are identified by minimisation of an objective function for residual errors of the marker positions $J = \frac{1}{2N}\sum_{n=1}^{N}\sum_{\beta=1}^{3}\left\|\boldsymbol{m}_\beta^2|_n - \overline{\boldsymbol{m}}_\beta^2|_n\right\|^2$. The results for parameter identification are evaluated by comparing these function values after optimisation.

Results To compare the simulation for cardan with respect to nino joint, for one sequence of $N = 40$ measurement frames the values for objective function J are shown below. The sequences are also evaluated for every second frame, thus $N = 20$ frames:

Joint type	N	J
cardan	40	0.0102
cardan	20	0.0101
nino	40	0.0057
nino	20	0.0058

It can be seen that the values for the nino joint are smaller than for cardan joint, assessing the nino joint as a more appropriate choice. Skipping every second frame within the observed sequence has a minor impairing effect on the results.

References

[1] S. Leyendecker, S. Ober-Blöbaum, J.E. Marsden, and M. Ortiz. *Discrete mechanics and optimal control for constrained systems.* Optimal Control Applications and Methods, 31:505-528, 2010.

[2] U. Phutane, M. Roller, S. Björkenstam, J. Linn and S. Leyendecker. *Kinematic validation of a human thumb model.* Proceedings of the ECCOMAS Thematic Conference on Multibody Dynamics, Prague, 2017.

[3] R. Maas. *Biomechanics and optimal control simulations of the human upper extremity.* PhD thesis. Friedrich-Alexander-Universität Erlangen-Nürnberg. 2014.

[4] J. Andersson, J. Gillis, G. Horn, J. Rawlings, and M. Diehl. *CasADi – A software framework for nonlinear optimisation and optimal control.* Mathematical Programming Computation. 2019.

[5] D. Winter. *Biomechanics and motor control of human movement.* Fourth Edition. 2009.

Discrete Cosserat rods

Holger Lang, Joachim Linn, Sigrid Leyendecker

The kinematics of a **continuous Cosserat rod** [2] is completely determined by its centerline $\boldsymbol{x} : [0, L] \to \mathbb{R}^3$ and a centerline fixed frame $\boldsymbol{R} = [\boldsymbol{d}^1, \boldsymbol{d}^2, \boldsymbol{d}^3] : [0, L] \to SO(3)$, which is specifying the cross section orientation with $\boldsymbol{d}^3$ being its normal. See Figure 2. With the strain $\boldsymbol{\Gamma} = \boldsymbol{R}^\top \partial_s \boldsymbol{x} - \boldsymbol{e}_3$ and the curvature $\boldsymbol{K} = \boldsymbol{R}^\top \partial_s \boldsymbol{R}$, the Hookean elasticity matrices $\boldsymbol{C}_\Gamma = \mathrm{diag}(GA, GA, EA)$ and $\boldsymbol{C}_K = \mathrm{diag}(EI_1, EI_2, GJ)$, and the generalised coordinates $\boldsymbol{q} = (\boldsymbol{x}, \boldsymbol{R})$, the total internal elastic energy can be expressed as

$$\mathcal{V} = \int_0^L \mathcal{W}(\boldsymbol{q}, \boldsymbol{q}')\mathrm{d}s, \qquad \mathcal{W}(\boldsymbol{q}, \boldsymbol{q}') = \frac{1}{2}\boldsymbol{\Gamma}^\top \boldsymbol{C}_\Gamma \boldsymbol{\Gamma} + \frac{1}{2}\boldsymbol{K}^\top \boldsymbol{C}_K \boldsymbol{K}.$$

In analogy of Lagrangian dynamic systems, $\mathcal{V}$ can be interpreted as the action, $\mathcal{W}$ as the Lagrangian function of the system. Forces and moments are related via $\boldsymbol{f} = \boldsymbol{R}\boldsymbol{C}_\Gamma\boldsymbol{\Gamma}$ resp. $\boldsymbol{m} = \boldsymbol{R}\boldsymbol{C}_K\boldsymbol{K}$ to the strain resp. curvature.

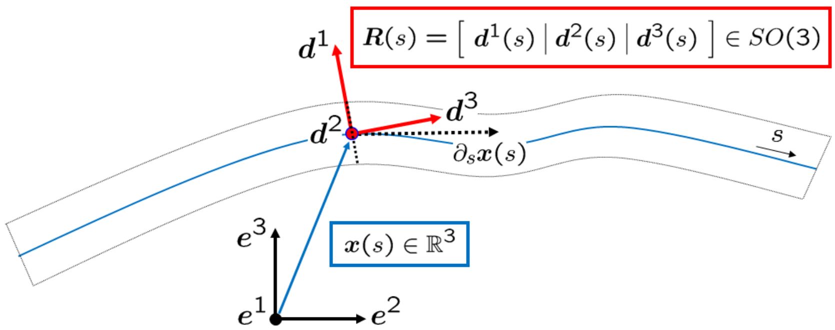

Figure 2: Kinematics of a Cosserat rod

The stationarity of the action functional (Hamilton's principle) leads to the continuous static equilibrium equations

$$\left\{ \begin{array}{rcl} \boldsymbol{0} &=& \boldsymbol{T}(\boldsymbol{q})^\top \left\{ \dfrac{\mathrm{d}}{\mathrm{d}s} \boldsymbol{\nabla}_{\boldsymbol{q}'} W(\boldsymbol{q}, \boldsymbol{q}') - \boldsymbol{\nabla}_{\boldsymbol{q}} W(\boldsymbol{q}, \boldsymbol{q}') \right\} \\ \boldsymbol{0} &=& \boldsymbol{g}(\boldsymbol{q}) \end{array} \right. ,$$

where $\boldsymbol{T}(\boldsymbol{q})$ is a null space matrix to the constraint function $\boldsymbol{g}(\boldsymbol{R}) = \boldsymbol{R}^\top \boldsymbol{R} - \boldsymbol{E}$, see e.g. [2].
The Noether Theorem [1] yields the following conserved magnitudes: The total force $\boldsymbol{f}(s)$ (since $\mathcal{W}$ is translatory invariant), the total momentum $\boldsymbol{m}(s) + \boldsymbol{x}(s) \times \boldsymbol{f}(s)$ (since $\mathcal{W}$ is rotatory invariant) and the twist moment $\langle \boldsymbol{m}(s), \boldsymbol{d}^3(s) \rangle$ (in case that $\mathcal{W}$ is isotropic, i.e., if $EI_1 = EI_2$). Here, $s \in [0, 1]$.

Similarly as in [2], a consistent **discrete Cosserat rod** can be defined by the discrete centroids $\boldsymbol{x}_n \in \mathbb{R}^3$ and discrete cross section orientations $\boldsymbol{R}_n \in SO(3)$, both situated on a discrete node (or vertex) grid $0 = s_0 < s_1 < \ldots s_N = L$. With the discrete strains $\boldsymbol{\Gamma}_\nu = \frac{1}{2\Delta s_\nu}(\boldsymbol{R}_{\nu-\frac{1}{2}} + \boldsymbol{R}_{\nu+\frac{1}{2}})^\top (\boldsymbol{x}_{\nu+\frac{1}{2}} - \boldsymbol{x}_{\nu-\frac{1}{2}}) - \boldsymbol{e}_3$ and the discrete curvatures $\hat{\boldsymbol{K}}_\nu = \frac{1}{\Delta s_\nu} \mathrm{inv\,cay}(\boldsymbol{R}^\top_{\nu-\frac{1}{2}} \boldsymbol{R}_{\nu+\frac{1}{2}})$, where $\Delta s_\nu = s_{\nu+1/2} - s_{\nu-1/2}$ and $\nu = \frac{1}{2}, \ldots, N - \frac{1}{2}$, the discrete internal elastic energy can be written as

$$V = \sum_{\nu=1/2}^{N-1/2} W_\nu \Delta s_\nu, \qquad W_\nu = \frac{1}{2}\boldsymbol{\Gamma}_\nu^\top \boldsymbol{C}_\Gamma \boldsymbol{\Gamma}_\nu + \frac{1}{2}\boldsymbol{K}_\nu^\top \boldsymbol{C}_K \boldsymbol{K}_\nu.$$

The stationarity of this discrete action (discrete Hamilton's principle) leads to the discrete static equilibrium equations

$$\left\{\begin{array}{rcl} \mathbf{0} & = & \boldsymbol{T}(\boldsymbol{q}_n)^\top\{\boldsymbol{\nabla}_l W(\boldsymbol{q}_n,\boldsymbol{q}_{n+1}) \;+\; \boldsymbol{\nabla}_r W(\boldsymbol{q}_{n-1},\boldsymbol{q}_n)\} \\ \mathbf{0} & = & \boldsymbol{g}(\boldsymbol{q}_n) \end{array}\right. ,$$

where $\boldsymbol{\nabla}_l$ resp. $\boldsymbol{\nabla}_r$ denote the gradient w.r.t. the left resp. right argument. Forces and momenta are obtained via the discrete Legendre transformation

$$\begin{bmatrix} \boldsymbol{f}_n \\ \boldsymbol{m}_n \end{bmatrix} = -\begin{bmatrix} \boldsymbol{E} & \\ & \boldsymbol{T}(\boldsymbol{q}_n)^\top \end{bmatrix} \boldsymbol{\nabla}_l W(\boldsymbol{q}_n,\boldsymbol{q}_{n+1}) = \begin{bmatrix} \boldsymbol{E} & \\ & \boldsymbol{T}(\boldsymbol{q}_n)^\top \end{bmatrix} \boldsymbol{\nabla}_r W(\boldsymbol{q}_{n-1},\boldsymbol{q}_n).$$

The discrete Noether Theorem [1] now yields the following conserved magnitudes: The total force $\boldsymbol{f}_n$ (since W is translatory invariant), the total momentum $\boldsymbol{m}_n + \boldsymbol{x}_n \times \boldsymbol{f}_n$ (since W is rotatory invariant) and the twist moment $\langle \boldsymbol{m}_n, \boldsymbol{d}_n^3 \rangle$ (in case that W is isotropic). Here $n = 0, 1, 2, \ldots, N$. See Figure 3 for the conserved quantities for a scenario, where the boundary conditions $\boldsymbol{x}_0 = \mathbf{0}$, $\boldsymbol{R}_0 = \boldsymbol{E}$,

$$\boldsymbol{x}_N = \begin{bmatrix} \frac{1}{5} \\ -\frac{1}{10} \\ \frac{4}{5} \end{bmatrix}, \qquad \boldsymbol{R}_N = \begin{bmatrix} \cos\frac{6}{5}\pi & 0 & \sin\frac{6}{5}\pi \\ \sin\frac{6}{5}\pi & 0 & -\cos\frac{6}{5}\pi \\ 0 & 1 & 0 \end{bmatrix}$$

are imposed and the parameters $L = 1$, $EI_1 = EI_2 = GJ = 1$, $GA = EA = 200$ are used. $N = 100$ elements are chosen.

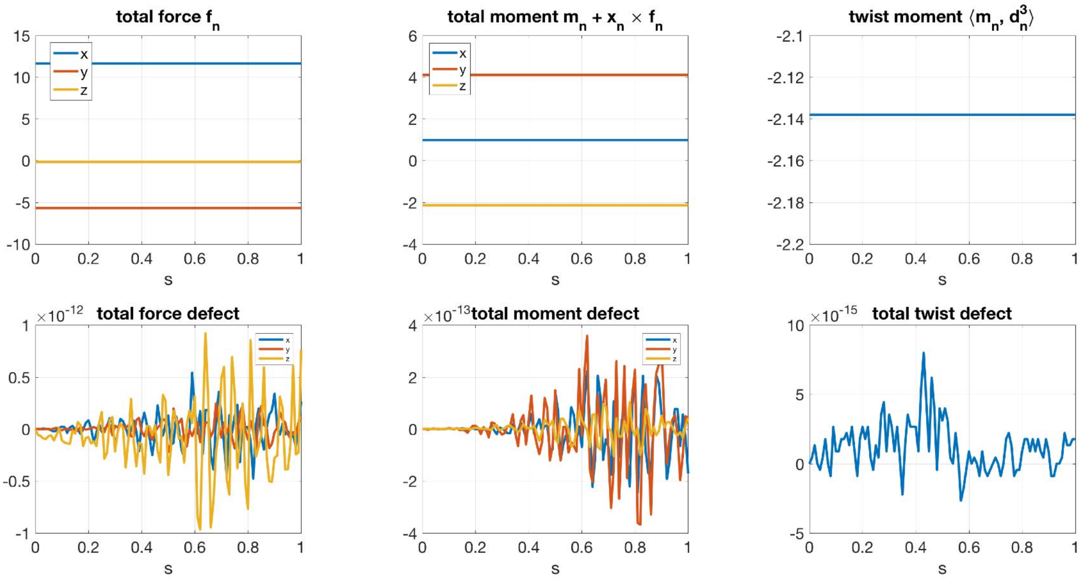

Figure 3: Above: Perfect conservation of the total force, the total moment and the twist moment. Below: The defects are of maximum order 10^{-12}.

References

[1] J. E. Marsden, M. West, "Discrete mechanics and variational integrators", *Acta Numerica*, Vol. 10, pp. 357-514, 2001.

[2] P. Jung, S. Leyendecker, J. Linn, M. Ortiz, "A discrete mechanics approach to the Cosserat rod theory - Part 1: static equilibria", *Int. J. Numer. Meth. Engng.*, Vol. 85, pp. 31-60, 2009.

Characterisation of passive mechanical properties of healthy and infarcted rat myocardium

Denisa Martonová, Julia Seufert[2], David Holz, Minh Tuan Duong, Muhannad Alkassar[2], Sigrid Leyendecker

During the cardiac cycle, electrophysiology is coupled with mechanical response of the myocardium. Beside the active contraction, passive mechanics plays an important role and its behaviour can differ in healthy and diseased hearts. To understand the normal and pathological physiology, laboratory rats are widely used as experimental animals. Supporting the animal testing, mathematical models and computational simulations can help these investigations and eventually lead to the development of medical devices supporting hearts with insufficiency, e.g. after myocardial infarction. However, these models crucially depend on the choice of parameters. There is a number of parameter sets obtained by calibrating a material model for cardiac tissue with mechanical experiments in different species – porcine, human, canine. They yield species-specific mechanical behaviour of the myocardium. For the rat left ventricle (LV), only few experimental data is available. Therefore, we focus on the identification of the passive material parameters in the healthy and infarcted rat LV by means of mechanical testing and subsequently parameter fitting. We performed uniaxial tensile tests on the healthy and infarcted myocardium from a rat LV in circumferential and radial direction. In order to identify material parameters which fit to different loading modes, our uniaxial tests are combined with other previously published tests in the rats – shear tests on the healthy myocardium [1] and equibiaxial tests on the infarcted tissue [4]. In a first step, we characterize the healthy rat LV by calibrating the anisotropic Holzapfel-Ogden strain energy function, see [3]

$$\Psi^m = \frac{a}{2b}\exp[b(I_1-3)] + \sum_{i=f,s}\frac{a_i^m}{2b_i^m}\left[\exp\{b_i^m\,(I_{4i}^m-1)^2-1\}\right] + \frac{a_{fs}}{2b_{fs}}\left[\exp\{b_{fs}\,(I_{8fs})^2\}-1\right], \qquad (1)$$

where a, b, a_i, b_i, for $i = s, f$ and a_{fs}, b_{fs} are material constants; I_3, I_{4i}, and I_{8fs} are the invariants of the right Cauchy-Green tensor. In a second step, the infarcted tissue is modelled as a mixture of intact myocardium and fibrotic scar structure, see Figure 1 right. Therefore, the strain energy function is decoupled in the form

$$\Psi = (1-fib)\,\Psi^m + fib\,\Psi^s, \qquad (2)$$

where the scar structure is modelled as an transversely isotropic material with the strain energy

$$\Psi^s = \frac{a^s}{2b^s}\exp\{b^s(I_1-3)\} + \frac{a_f^s}{2b_f^s}\left[\exp\{b_f^s\,(I_{4f}^s-1)^2\}-1\right]. \qquad (3)$$

The amount of fibrosis fib obtained from the histology serves as a scaling factor as we found a positive correlation between the tensile moduli computed from the slope in the steepest region of individual stress-strain curves and the amount of fibrosis.

With parameters obtained from fitting, we test a finite element model (FEM) during the passive end-diastolic filling by applying a pressure boundary condition on the inner surface of the rat LV model generated from magnetic resonance imaging, see Figure 2 right. The pressure-volume relation is compared in the model with our new parameters for the healthy and infarcted case and previously used passive material parameters in [2]. In our mechanical experiments, we observed significantly different tensile moduli in the healthy and infarcted samples, see Figure 1. Similar difference is observed in the finite element simulation regarding pressure-volume relation during the end-diastolic filling. On the other hand, in the heathy case, the pressure-volume relation for the model with our new and previous parameters shows nearly identical behaviour, see Figure 2 left.

[2]Pediatric Cardiology, Friedrich-Alexander-Universität Erlangen-Nürnberg, 91054 Erlangen, Germany

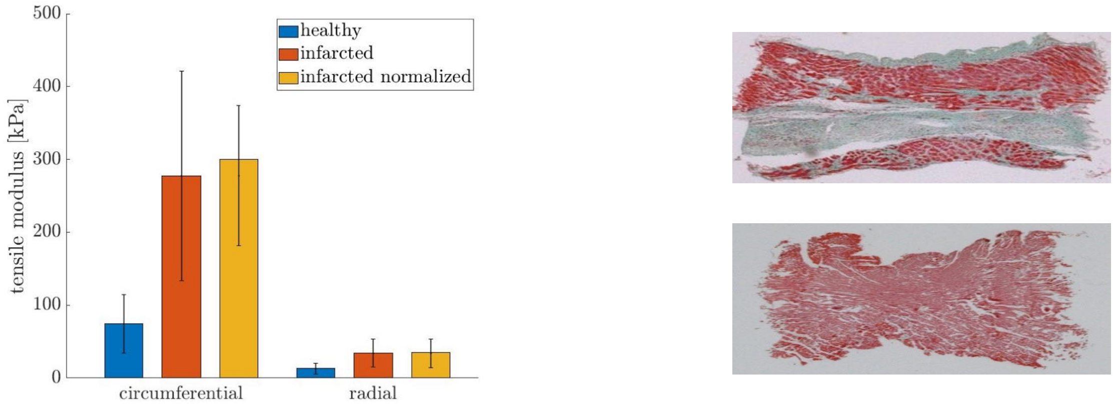

Figure 1: Left: circumferential and radial tensile modulus in healthy, infarcted and normalized group (mean ± SD). The normalisation is with respect to the average amount of fibrosis. Right: histological images of infarcted (upper) and healthy (lower) myocardium.

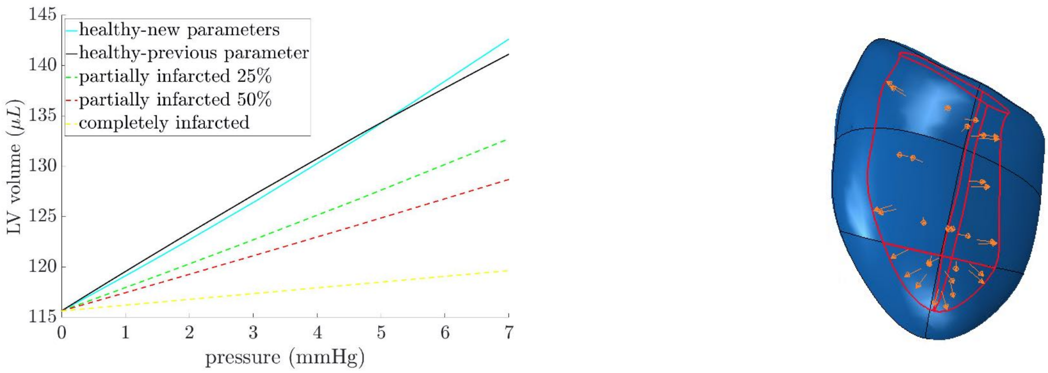

Figure 2: Comparison of different passive material models in the FEM of the rat LV. Left: pressure-volume relation in end-diastolic filling. Right: NURBS model of rat LV with applied pressure boundary condition on the inner ventricular surface.

Acknowledgments This work is funded by the Klaus Tschira Stiftung grant 00.289.2016.

References

[1] S. Dokos, I. J. LeGrice, B. H. Smaill, J. Kar, and A. A. Young. *A Triaxial- Measurement Shear-Test Device for Soft Biological Tissues.* Journal of Biomechanical Engineering **122(5)**, 471 (2000).

[2] M. T. Duong, D. Holz, M. Alkassar, S. Dittrich, and S. Leyendecker. *Interaction of the Mechano-Electrical Feedback With Passive Mechanical Models on a 3D Rat Left Ventricle: A Computational Study.* Frontiers in Physiology **10,** 1041 (2019).

[3] G.A. Holzapfel, and R.W. Ogden. *Constitutive modelling of passive myocardium: a structurally based framework for material characterisation.* Phil. Trans. R. Soc. A. **367**, 3445–3475 (2009).

[4] M. S. Sirry, J. R. Butler, S. S. Patnaik, B. Brazile, R. Bertucci, A. Claude, R. McLaughlin, N. H. Davies, J. Liao, and T. Franz. *Characterisation of the mechanical properties of infarcted myocardium in the rat under biaxial tension and uniaxial compression.* Journal of Mechanical Behavior of Biomedical materials **63**, 252–264 (2016).

Biomechanical simulations with dynamic muscle paths on NURBS surfaces

Johann Penner, Sigrid Leyendecker

When simulating musculoskeletal motion with multibody systems representing bones and joints, the muscle paths are highly relevant for the muscle forces, moment arms and resulting body and joint loads. Typically, muscle paths cannot be adequately represented as straight lines because the anatomical structure of the human body forces the muscles to wrap around bones and adjacent tissue. Assuming that the muscles and tendons are always under tension, their path can be modelled as a locally length minimizing curve that wraps smoothly over adjacent obstacles [1]. Due to the complex geometry of bones and tissue, the determination of muscle paths is very challenging. To model these wrapping obstacles in this work, the widely used and well known mathematical model of NURBS surfaces [4] is used to create and display arbitrary surfaces.

Within this work, the muscle path is modeled as the shortest connection between two points on dynamic obstacle surfaces. Assuming that the muscle completely touches the surface, the Lagrangian is augmented by a scalar valued function of holonomic surface constraints $\phi(\boldsymbol{\gamma}) = 0 \in \mathbb{R}$ and a Lagrange multiplier $\lambda \in \mathbb{R}$. Furthermore, the action is given by a scalar functional $E[\boldsymbol{\gamma}, \lambda] = \int_{s_0}^{s_K} \left(\frac{1}{2} \parallel \boldsymbol{\gamma}'(s) \parallel^2 - \phi(\boldsymbol{\gamma}) \cdot \lambda \right) \mathrm{d}s$ of a curve $\boldsymbol{\gamma} \in C^2([s_0, s_K], \mathbb{R}^3)$ from start point $\boldsymbol{\gamma}(s_0)$ to the end point $\boldsymbol{\gamma}(s_K)$. The local minimizers of E, which also locally minimize the length, are the so called geodesics [3]. The variational principle $\delta E = 0$ yields that for a stationary point $\boldsymbol{\gamma}$ of E,

$$\begin{aligned} \frac{\mathrm{d}}{\mathrm{d}s}\frac{\partial \mathcal{L}(\boldsymbol{\gamma}')}{\partial \boldsymbol{\gamma}'} + \boldsymbol{\Phi}(\boldsymbol{\gamma})^T \cdot \lambda &= \mathbf{0} \\ \phi(\boldsymbol{\gamma}) &= 0 \end{aligned} \tag{1}$$

$$\left[\frac{\partial \boldsymbol{F}(\boldsymbol{\nu})}{\partial \boldsymbol{\nu}}\right]^T \cdot \left[\frac{\mathrm{d}}{\mathrm{d}s}\frac{\partial \mathcal{L}(\boldsymbol{\gamma}')}{\partial \boldsymbol{\gamma}'}\right] = \mathbf{0} \tag{2}$$

the corresponding Euler-Lagrange equation (1) has to hold, where $\boldsymbol{\Phi}(\boldsymbol{\gamma}) = \partial\phi(\boldsymbol{\gamma})/\partial\boldsymbol{\gamma} \in \mathbb{R}^{1\times 3}$ is the surface constraint Jacobian and $\boldsymbol{\gamma}'$ is the derivative of the geodesic curve with respect to s. Given a nonsingular differentiable parametrization $\boldsymbol{\gamma} = \boldsymbol{F}(\boldsymbol{\nu})$ in terms of surface coordinates $\boldsymbol{\nu} \in \mathbb{R}^2$, the Jacobian $\partial \boldsymbol{F}(\boldsymbol{\nu})/\partial\boldsymbol{\nu} \in \mathbb{R}^{3\times 2}$ can be used to project equation (1) into the tangent space of the manifold defined by the surface constraint. Thus, differential equation (2) is equivalent to equation (1) and the Jacobian $\partial \boldsymbol{F}(\boldsymbol{\nu})/\partial\boldsymbol{\nu}$ plays the role of a null space matrix. From the point of view of classical mechanics, the solution of equations (1) and (2) is the trajectories of a free particle on a constraint manifold. In fact, this means that the acceleration vector $\frac{\mathrm{d}}{\mathrm{d}s}\partial\mathcal{L}(\boldsymbol{\gamma}')/\partial\boldsymbol{\gamma}'$ of the curve has no components in the normal direction of the surface and the motion is entirely determined by the surface curvature.

As a practical example, the lifting of the human arm from an outstretched initial configuration to a flexed elbow is examined. The multibody configuration $\boldsymbol{q} \in \mathbb{R}^{24}$ consist of two rigid bodies, which represent the upper and lower arm. For simplicity, a revolute joint is used to model the elbow and the upper arm is fixed in space. Given a control net $\boldsymbol{B}_{ij}(\boldsymbol{q})$ with $n \times m$ control points as function of the configuration $\boldsymbol{q}$, polynomial orders k and l, the knot vectors $\boldsymbol{u} = [u_0, u_1, ..., u_{n+k+1}]$ and $\boldsymbol{v} = [v_0, v_1, ..., v_{m+l+1}]$, a NURBS surface is given by the tensor product

$$\boldsymbol{F}(u, v) = \sum_{i=1}^{n}\sum_{j=1}^{m} \boldsymbol{B}_{ij}(\boldsymbol{q})\boldsymbol{N}_{ij}(u, v) \tag{3}$$

where $\boldsymbol{N}_{ij}(u, v)$ are the so-called rational basis functions, see [4]. By coupling the control network with the configuration, the NURBS surface moves together with the multibody system, forming a closed wrapping surface for all muscles. Fig. 1 shows the implemented exemplary wrapping surfaces for the biceps and the triceps. Moreover, the evolution of the muscle length is shown for two different wrapping formulations. On the left hand side, the bone geometry is approximated via a NURBS surface, while the muscles in the centre wrap around several cylinders and spheres with G1-continuous transitions. The geometry of this example should be understood as a theoretical example and is not based on real anatomy data. However, the evolution of muscle lengths for the biceps and triceps shows qualitatively the same behaviour.

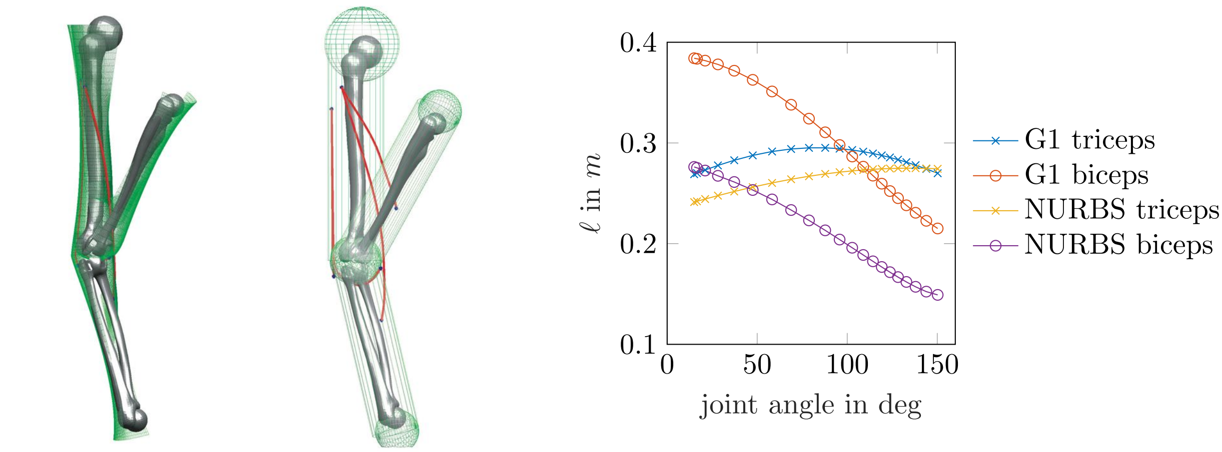

Figure 1: **Left:** Muscle path of the biceps and the triceps around NURBS bone geometry approximation and a multiple obstacle formulation. **Right:** Length evolution of the biceps and triceps for two different wrapping surfaces.

This work shows a muscle wrapping formulation on dynamic NURBS surfaces. The shortest connection between two points on an obstacle surface is derived using constrained variational dynamics. This allows to constrain the muscle path to arbitrarily complex obstacle surfaces, which can be represented by the well-known NURBS description. In the given example, the evolution of the muscle length and orientation shows the same qualitative behaviour as in widely used multi obstacle wrapping methods, see e.g. [1]. The major difference is that the wrapping obstacle is modeled as a single closed surface and no calculation of G1-continuous transitions is necessary. Due to this, we expect that this formulation is well suited to be used in more complex musculoskeletal models, which is our next step.

Acknowledgments This work is funded by the Federal Ministry of Education and Research (BMBF) as part of the project 05M16WEB - DYMARA.

References

[1] A. Scholz, M. Sherman, I. Stavness, S. Delp and A. Kecskemethy. A fast multi-obstacle muscle wrapping method using natural geodesic variations. Multibody System Dynamics **36**(2):195–219, 2016.

[2] R. Maas and S. Leyendecker. Biomechanical optimal control of human arm motion. Proceedings of the Institution of Mech. Eng., Part K: J. of Multi-body Dyn. **227**(4):375–389, 2013.

[3] H. Thielhelm, A. Vais, D. Brandes and F. E. Wolte. Connecting geodesics on smooth surfaces. The visual computer **28**, 529–539, 2012.

[4] L. Piegl, W. Tiller. The NURBS book. Springer Science & Business Media, 2012.

Challenges associated with quasi-static phase-field model for brittle fracture

Dhananjay Phansalkar, Sigrid Leyendecker

The existence of micro-cracks and flaws further leading to fracture cannot be prevented in engineering structures. The requirement for an accurate estimate for the failure of load-bearing components of all kinds is evident. Traditionally, cracks are studied as an evolving internal discontinuous boundary $\Gamma(t)$, that represents a discrete crack. Alternatively, a phase-field model represents, the fracture as a smooth interface between broken and undamaged material, namely a diffusive crack. According to Griffith's theory of fracture, the energy needed to construct a fracture surface unit area is equal to the critical energy density of the fracture $\mathcal{G}_c$. The total potential energy of the body $\mathcal{E}$, is the sum of the elastic energy ψ_e and the fracture energy, given by $\mathcal{E}(\boldsymbol{u},\Gamma) = \int_\Omega \psi_e\left(\boldsymbol{\varepsilon}(\boldsymbol{u})\right)\mathrm{d}\mathbf{x} + \int_\Gamma \mathcal{G}_c \mathrm{d}\mathbf{x}$. Instead of applying the classical Griffith criterion to predict the evolution of crack, a variational formulation of the model is proposed in [1]. In order to make this variational formulation suitable for numerical implementation, [3] proposes a regularized version of this variational formulation and it reads

$$E(\boldsymbol{\varepsilon}(\boldsymbol{u}),c) = \int_\Omega (c^2+\eta)\psi_e(\boldsymbol{\varepsilon}(\boldsymbol{u}))\mathrm{d}\mathbf{x} + \frac{\mathcal{G}_c}{4}\int_\Omega \left(\frac{(1-c)^2}{\epsilon} + \epsilon|\nabla c|^2\right)\mathrm{d}\mathbf{x}. \tag{1}$$

where $\boldsymbol{u}, c, \varepsilon$ and ϵ are the displacement, phase-field, strain and regularisation parameter respectively. It can be shown that this regularized formulation approximates the variational formulation of brittle fracture in the sense of Γ-convergence [4]. Minimizing the energy functional (1) with respect to $\boldsymbol{u}$ and c we obtain the following Euler-Lagrange equations

$$\begin{aligned} \nabla\cdot\boldsymbol{\sigma} &= \mathbf{0} \quad \text{in} \quad \Omega \\ \left[\frac{4\epsilon\psi_e(\boldsymbol{\varepsilon}(\boldsymbol{u}))}{\mathcal{G}_c} + 1\right] c - 4\epsilon^2\Delta c &= 1 \quad \text{in} \quad \Omega \end{aligned} \tag{2}$$

In addition to equations of motion (2), the typical boundary conditions for phase-field problem are $\boldsymbol{u} = \boldsymbol{u_0}$ on $\partial\Omega_\mathrm{d}$ and $\nabla c \cdot \boldsymbol{n} = 0$ on $\partial\Omega$. First, we restrict ourselves to a one-dimensional domain $\Omega \in (-L, L)$ to understand various characteristics of the phase-field formulation for brittle fracture. Figure 1 shows the problem configuration. The analytical solution of the phase-field for the above mentioned boundary value problem can be shown to be

$$x(c) = \int_{c_{crack}}^{c(x)} \left[\frac{\bar{c}^2}{2} - \bar{c} - \frac{\epsilon\sigma^2}{\mathbb{C}\mathcal{G}_c[\eta+\bar{c}^2]} + a\right] d\bar{c} \tag{3}$$

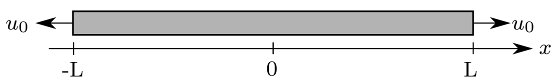

Figure 1: 1D problem set-up

Evaluating this integral numerically for stress $\sigma = \beta\sigma_c$ with various values of $\beta \in [0,1]$ and critical stress σ_c we get Figure 2a. Nonetheless, it is quite tricky to solve this 1D problem numerically using the non-linear finite element method. When we solve the equations (2) simultaneously, typically called a monolithic approach, the residual from the Newton method explodes even with very small load steps. We can reformulate the energy functional (1) with an additional evolution law. However, it does not resolve this convergence issue. It can be improved by damping the Newton update as suggested in [2]. This improvement is limited i.e., the residual decreases and then stagnates. Alternatively, the equations (2) can be solved one after the other for a fixed point solution; this is typically called a staggered approach. However, for all the load steps greater than the critical load the resulting solution does not coincide with the analytical solution. Also weakening the fracture toughness ($\mathcal{G}_c$) at the center does not help to obtain the predicted analytical solution.

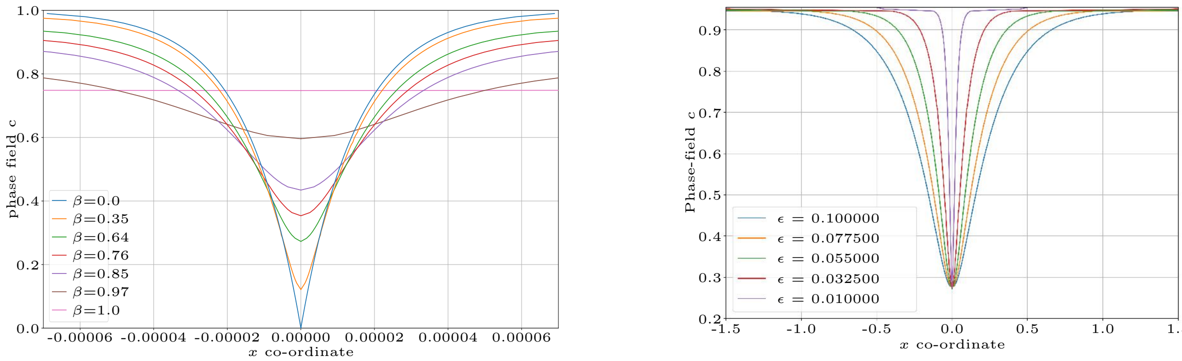

(a) Phase field solution for various values of the stress with $\epsilon = 7.5 \times 10^{-6}$

(b) Phase field solution for various values of the ϵ with $\beta = 0.64$

Figure 2: Analytical solution of the stationary evolution equation in 1D.

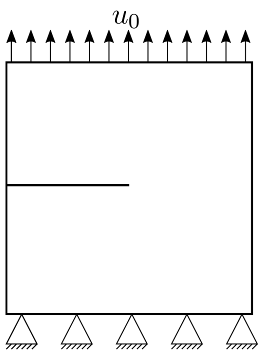

Figure 3: 2D problem set-up

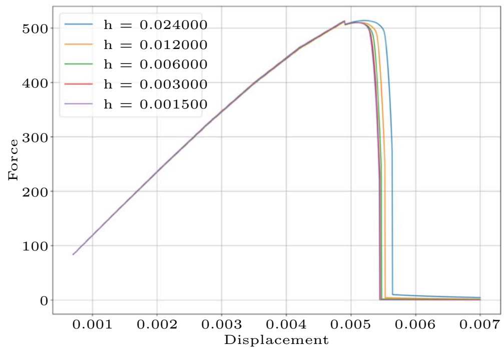

Figure 4: Force vs displacement with $\epsilon = 0.1$

These problems make it quite difficult to simulate the 1D problem. Hence we move on to a 2D problem with the set-up as depicted in Figure 3. We try to solve this problem with the staggered approach and study the behavior with respect to two parameters, ϵ and mesh size h. The force vs displacement plot Figure 4 provides a good measure to understand the behavior. This study also provides an upper bound for the mesh size with respect to regularization parameter i.e. $h = \epsilon/17$ to obtain a reliable solution.

Acknowledgement : The German Research Foundation (DFG) is gratefully acknowledged for funding this research within the research training group GRK2423 FRASCAL.

References

[1] G.A. Francfort and J.J. Marigo. *Revisiting Brittle Fracture as an Energy Minimization Problem.* Journal of the Mechanics and Physics of Solids, 46:1319-1342, 1998.

[2] T. Gerasimov and L. de Lorenzis. *A Line Search Assisted Monolithic Approach for Phase-Field Computing of Brittle Fracture.* Computer Methods in Applied Mechanics and Engineering, 312:276-303, 2016.

[3] B. Bourdin, G. Francfort and J.J. Marigo. *Numerical Experiments in Revisited Brittle Fracture.* Journal of the Mechanics and Physics of Solids. 48:797-826, 2000.

[4] L. Ambrosio, V.M. Tortorelli. *Approximation of Functional Depending on Jumps by Elliptic Functional via* Γ*-Convergence.* 43:999-1036, 1990.

Optimal control grasping simulations for objective specific contact points

Uday D. Phutane, Michael Roller[3], Sigrid Leyendecker

Introduction Grasping is a complex human activity which is performed with high dexterity and coordination. It is possible due to the complicated kinematic and dynamic nature of the hand. Grasping research has major implications in areas such as ergonomic tool development, industrial robotics, and assembly planning etc. We have demonstrated the method to solve an optimal control problem (ocp) for grasping in [4] to perform precision grasps. In [4], human-like grasping of an object with a three-dimensional, control joint torques actuated two-finger hand model with thirteen rigid bodies was reproduced for a variety of grasps and objectives. The ocp, essentially a constrained optimisation problem, can be expressed as a hybrid dynamical system to describe two sequential phases, namely a reaching phase to first close the contact and a grasping phase, to perform a grasp manoeuvre. However, the grasps therein were executed with prescribed contact points on the fingers. This severely limits the possibilities to execute more complicated grasps, as it would be challenging to prescribe contact points for more than two fingers with complex shapes.

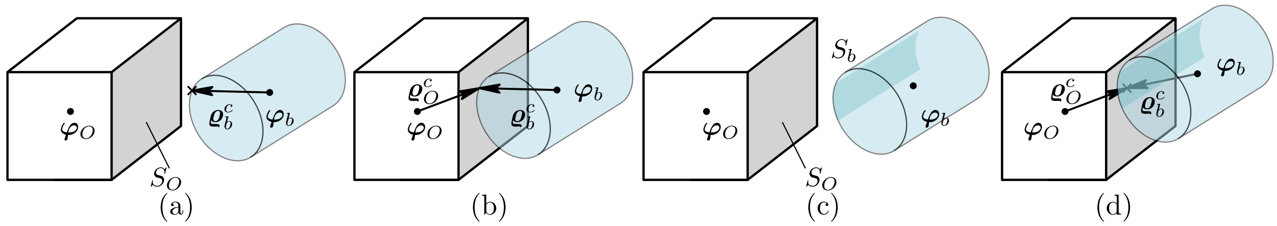

Figure 1: In (a) the c-th contact point $\boldsymbol{\varrho}_b^c$ for finger digit b is defined, then after contact closure with the object surface S_O, the calculation for point $\boldsymbol{\varrho}_O^c$ is straightforward (b). In (c) the components of $\{\varrho_O^c\}_i$ are optimisation variables which are constrained to lie on the shaded surface S_b. The closure constraint is applied as before and thereafter, $\boldsymbol{\varrho}_O^c$ and $\boldsymbol{\varrho}_b^c$ are determined (d).

Contact points as optimisation variables Consider a contact c between finger digit b and object O. Here, $b \in [1, n_b]$ and $c \in [1, n_c]$, where n_c the the total number of contacts between n_b bodies and the object. As in director formulation, see [1], the configuration for a rigid body $\alpha, \in \{1, \ldots, n_b, O\}$ is defined in redundant formulation as $\boldsymbol{q}_\alpha = [\boldsymbol{\varphi}_\alpha,\ \boldsymbol{d}_{1,\alpha},\ \boldsymbol{d}_{2,\alpha},\ \boldsymbol{d}_{3,\alpha}]$, with $\boldsymbol{\varphi}_\alpha$ as the body centroid, and $\{\boldsymbol{d}_{i,\alpha}\}_{i=1,2,3}$ as an orthonormal triad to represent the body orientation. A material point, e.g. the c-th contact point $\boldsymbol{\varrho}_c^b$, on the body b is expressed as $\sum_{i=1}^3 \{\varrho_b^c\}_i \boldsymbol{d}_{i,b}^c$ with respect to $\boldsymbol{\varphi}_b$, see Figure 1 (a). To close the contact c, we impose non-negative gap function constraints $\boldsymbol{g}_{c1}^c\,(\boldsymbol{q}_b, \boldsymbol{q}_O) = 0$ between $\boldsymbol{\varrho}_b^O$ and object surface S_O. The c-th contact point on the object, hitherto undefined and free to be chosen on the object surface, is thence determined during the contact closure. This is due to the fact that the c-th point global coordinates are shared by the object and the digit. The components of the c-th contact point on the object are therefore determined through $\{\varrho_O^c\}_i = (\boldsymbol{R}_O)^T \cdot (\boldsymbol{\varphi}_b^c + \boldsymbol{\varrho}_b^c - \boldsymbol{\varphi}_O^c)$ where $\boldsymbol{R}_O = [\boldsymbol{d}_{1,O},\ \boldsymbol{d}_{2,O},\ \boldsymbol{d}_{3,O}]$, as shown in Figure 1 (b). Following that, to perform the grasping action, we use spherical joint constraints $\boldsymbol{g}_{c2} = \boldsymbol{\varphi}_b^c + \boldsymbol{\varrho}_b^c - (\boldsymbol{\varphi}_O^c + \boldsymbol{\varrho}_O^c) = \boldsymbol{0}$, which restricts three relative translational displacements between the contact points on the finger and on the object to zero. This process of closing the grasp, determining the contact points $\{\varrho_O^c\}_i$, and the application of spherical joint constraints can also be implemented by additionally introducing the components $\{\varrho_b^c\}_i$ as solution variables in the optimisation problem. This must be supplanted by two sets of additional constraints, namely equality constraints to have the point $\boldsymbol{\varrho}_c^b$ on the surface of the digits and inequality constraints to limit the components to a specific area of the digit S_b, as shown in Figure 1 (c) and (d).

[3]Fraunhofer Institute for Industrial Mathematics, Kaiserslautern, Germany

Here, we compare the results from ocp simulations with the prescription of the components $\{\varrho_b^c\}_i$, i.e. the prescribed case, and their inclusion as solution variables in the optimisation problem, i.e. the free case. We perform optimal control simulations with two objectives, namely, minimising the distance between the object and the contact polygon centroids (J_1) and minimising the rate of change of control torques (J_2), see [4], with the values for the objectives expressed through J_{1v} and J_{2v}, respectively.

Results We present an example of rest-to-rest palmar pinch grasping. The palmar pinch grasp holds thin or thick objects such as a card, a dice or a ball. This is simulated with two contact points each on the index finger and the thumb distal phalanges. It is observed that the positions of contact points $\{\boldsymbol{\varrho}_b^c\}_{b=1,2}^{c=1,\cdots,4}$ on the fingers for the free case are similar across the two objectives and two cases, with a notable exception observed for the index finger digit for J_{2v} objective, as shown in Fig. 2. The distances $J_{1,d}$ for the ocp with J_1 objective are numerically zero in the prescribed and free cases. For the ocp with J_{2v}, the distance $J_{1,d}$ in the free case is higher than in the prescribed case. Interestingly, the ocp with J_2 objective, finds a totally different minimum to lift the object with the side of the index finger digit, instead of the pulp.

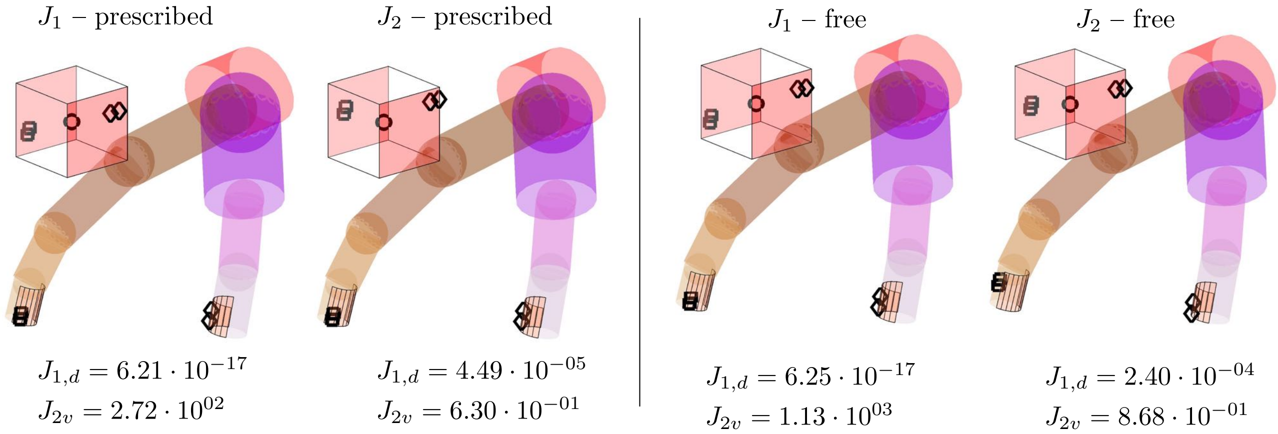

Figure 2: The contact points for the palmar pinch grasps for the simulations with prescribed and free contact points for the ocp with objectives J_1 and J_2. The distance $J_{1,d}$ and torque change value J_{2v} from the objective functions, are provided below every picture. The contact points for the thumb and the finger are shown with ($\Diamond$) and ($\Box$) markers, respectively.

Acknowledgements This work is supported by the Fraunhofer Internal Programs under Grant No. MAVO 828424.

References

[1] S. Leyendecker, S. Ober-Blöbaum, J.E. Marsden, and M. Ortiz. Discrete mechanics and optimal control for constrained systems. Optimal Control Applications and Methods, 31:505-528, 2010.

[2] Roa, M A, and Suárez, R Grasp quality measures: review and performance. Autonomous Robots. 38:65–88, 2014.

[3] U. Phutane, M. Roller, S. Björkenstam, J. Linn and S. Leyendecker. Kinematic validation of a human thumb model. Proceedings of the ECCOMAS Thematic Conference on Multibody Dynamics, Prague, 2017.

[4] U. Phutane, M. Roller, and S. Leyendecker. Optimal control simulations of lateral and tip pinch grasping. Proceedings of the ECMI Conference, Budapest, 2018.

High order variational integrators in constrained mechanical problems and field theories

Rodrigo T. Sato Martín de Almagro, Sigrid Leyendecker

Mechanical and field theoretical systems model the evolution of physical objects, from tiny specks of dust or the bending of a reed to atmospheric phenomena or the overall cosmological structure of the universe. The accurate numerical simulation of such systems has important applications both in the theoretical and applied realms. Such systems display important qualitative features that should ideally be present in the results of a simulation, such as conservation of quantities due to symmetries in the system (Noether's theorem) or the compliance with specified constraints.

Mathematically, many of these systems can be described at a fundamental level as extremisation problems in certain spaces. These types of problems are called *variational*, where the basic set-up is a given space, e.g. the space of all the curves lying on a surface with fixed ends, and a certain measure of the quality or cost of such curve. The solution of a variational problem entails singling out curves such that when slightly perturbed (varied) the cost varies negligibly. Then, it is said that the cost has attained a stationary value.
Variational integrators [1] are numerical methods to integrate such systems that mimic the same procedure in simplified spaces. It has been proven that such methods can preserve some of the most salient features of the original problems, contrary to other classical approaches.

We focus on constructing variational integrators with proven accuracy (covergence rates) for such systems, often in the presence of constraints. Constraints can make the system preserve its variational structure or lose it, depending on the type. Of the former type are *holonomic* constraints (integrable), involving only the configuration of the system, while of the latter we have *nonholonomic* constraints (non-integrable), involving also the velocities, such as a objects rolling without sliding. Even if the latter type of systems stops being purely variational, the substrate of the underlying theory still has its roots in the variational realm, so it still makes sense to treat the systems in a similar fashion, though it is not immediately clear how to do so.
Currently there are several problems we are researching:

- We are continuing the work of Thomas Leitz [3, 5] on projected Galerkin integration applied to certain geometric structures called Lie groups. This type of integration allows us to work on these complicated spaces as constrained problems. We consider two particular Lie groups that appear frequently in engineering applications: the group of rotations in 3D, $SO(3)$, and the Euclidean group in 3D, $SE(3)$, which includes the former as well as translations. In these cases it is possible to consider these groups as immersed in particularly well-suited ambient spaces, leading to constrained problems. These are the space of *quaternions* and the space of *dual quaternions* respectively, which are equipped with their own products but, crucially, compatible with the group operations of our groups. Furthermore, interpolation in these ambient spaces can be performed nearly effortlessly, which has led to earlier uses of these as tools in areas such as computer animation. The model we are considering here is the geometrically exact beam [4, 2], which is important in modelling slender structures (see fig. 1).

- We are studying high-order collocation-based methods for variational field theories in triangular meshes. In 1D, collocation methods are integration methods where a polynomial approximation is asked to satisfy the corresponding differential equation at a finite set of *collocation* points. In 2D or higher, these can be readily extended in structured domains (rectangular meshes) as tensor product rules. The case of unstructured meshes of triangular elements (fig. 2) does not

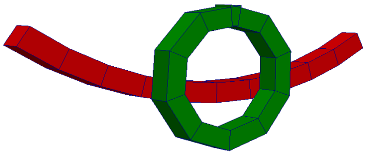

Figure 1: Two geometrically exact beams under the same load. The red one displays shear-lock, appearing stiffer than the green one.

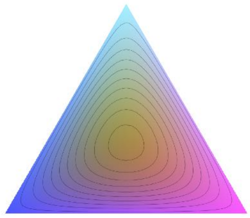

Figure 2: Single element 10-point Lobatto integration of the Poisson equation with unit source term in an equilateral triangle. The method is exact for general polynomials in 2 variables of order 3 and the solution of the problem turns out to be one such polynomial, so the integration is exact.

seem to have been well-explored in the literature in favour of easier to implement and understand Galerkin methods. However, collocation methods are devoid of certain numerical artifacts that Galerkin methods can display (such as shear-lock, fig. 1), they can give us sharper accuracy estimates and have interesting consequences as to the interpretation of the discrete version of a theory.

- We are also studying how to generate mesodynamical integrators in collaboration with prof. M. Ortiz, where we are integrating the field equations of a density on phase space. The equation governing the evolution of such density is Lioville's equation, which are the equations of an incompressible fluid whose velocity field coincides with the Hamiltonian vector field of the system under consideration.
- Finally, we are also interested in extending the construction of nonholonomic collocation methods in [6] to Galerkin methods. This might lead to easier construction of nonholonomic integrators.

References

[1] J. Marsden and M. West. *Discrete mechanics and variational integrators.* Acta Numerica, (10):357–514, 2003.

[2] F. Demoures, F. Gay-Balmaz, S. Leyendecker, S. Ober-Blöbaum, T. Ratiu and Y. Weinand. *Discrete variational Lie group formulation of geometrically exact beam dynamics.* Numer.Math.,(130):73–123, 2015.

[3] T. Leitz and S. Leyendecker. *Galerkin Lie-group variational integrators based on unit quaternion interpolation.* Comput. Methods Appl. Mech. Engrg., (338):333–361, 2018.

[4] J.C. Simo. *A finite strain beam formulation. The three-dimensional dynamic problem. Part I.* Comput. Methods Appl. Mech. Engrg., (49):55–70, 1985.

[5] T. Leitz and S. Leyendecker. *Towards higher order multi-symplectic Lie-group variational integrators for geometrically exact beam dynamics – avoidance of shear locking.* In Proceedings of the 8th ECCOMAS Thematic conference on Mutibody Dynamics, 2017.

[6] R.T. Sato Martín de Almagro. *Convergence of Lobatto-type Runge-Kutta methods for partitioned differential-algebraic systems of index 2.* pre-print `arXiv:1810.10298`, submitted 10,2018.

A predeformed geometrically exact beam model for a dynamic-response prosthesis

Eduard S. Scheiterer, Sigrid Leyendecker

Clinical trials have shown that the storage and release of energy in prosthetic feet plays a major role in the resulting walking comfort for the patient. In comparison to rigid multi-axis prosthetic feet, dynamic-response prosthetic feet (e.g. the Össur Vari-Flex® used in this work) show good energy storage and release capabilities and thereby increase the walking comfort of the patient. To accurately simulate such a prosthesis in a gait cycle simulation, its model has to represent the deformation energy as accurately as possible.

In the following, the prosthetic foot is modelled as a predeformed geometrically exact beam, based on the theory from [1, 2]. A St. Venant-Kirchhoff-type stored energy function is used to describe the internal deformation energy

$$W_{int}(\mathbf{\Gamma}, \boldsymbol{K}) = \frac{1}{2}\mathbf{\Gamma}^T \cdot \boldsymbol{D}^\Gamma \cdot \mathbf{\Gamma} + \frac{1}{2}\boldsymbol{K}^T \cdot \boldsymbol{D}^K \cdot \boldsymbol{K}. \tag{1}$$

This function describes an ideally elastic material behaviour, similar to Hook's law for simple elastic material. It uses the material specific parameter matrices

$$\boldsymbol{D}^\Gamma = \begin{bmatrix} GA_1 & 0 & 0 \\ 0 & GA_2 & 0 \\ 0 & 0 & EA \end{bmatrix} \quad \text{and} \quad \boldsymbol{D}^K = \begin{bmatrix} EI_1 & 0 & 0 \\ 0 & EI_2 & 0 \\ 0 & 0 & GJ \end{bmatrix}, \tag{2}$$

consisting of the Young's modulus E, the shear modulus G and geometry specific parameters e.g. the cross-section area A. The effective cross-section areas $A_1 = \kappa_1 A$, $A_2 = \kappa_2 A$ counteract shear-locking effects with the Timoshenko shear correction factors $0 < \kappa_1, \kappa_2 \leq 1$. The other parameters are the area moments of inertia I_1, I_2 and the polar moment of inertia J. The strain measures $\mathbf{\Gamma}(\boldsymbol{q}) = \Gamma_i \boldsymbol{e}_i$ and $\boldsymbol{K}(\boldsymbol{q}) = K_i \boldsymbol{e}_i$ with

$$\Gamma_i = \boldsymbol{d}_i^T \cdot \frac{\mathrm{d}}{\mathrm{d}s}\boldsymbol{\varphi} - [\boldsymbol{d}_i^T \cdot \frac{\mathrm{d}}{\mathrm{d}s}\boldsymbol{\varphi}]\Big|_{t_0} \text{ and } K_i = \frac{1}{2}\epsilon_{ijk}\left[\boldsymbol{d}_k^T \cdot \frac{\mathrm{d}}{\mathrm{d}s}\boldsymbol{d}_j - [\boldsymbol{d}_k^T \cdot \frac{\mathrm{d}}{\mathrm{d}s}\boldsymbol{d}_j]\Big|_{t_0}\right], \quad i, j, k = 1, 2, 3, \tag{3}$$

quantify shear ($\Gamma_{1,2}$), elongation (Γ_3), flexion ($K_{1,2}$) and torsion (K_3), respectively. Figure 1 visualises the continuous formulation of a geometrically exact beam on the left, while the right side shows the resulting model of the prosthesis from [3, 4] in a undeformed and deformed state.

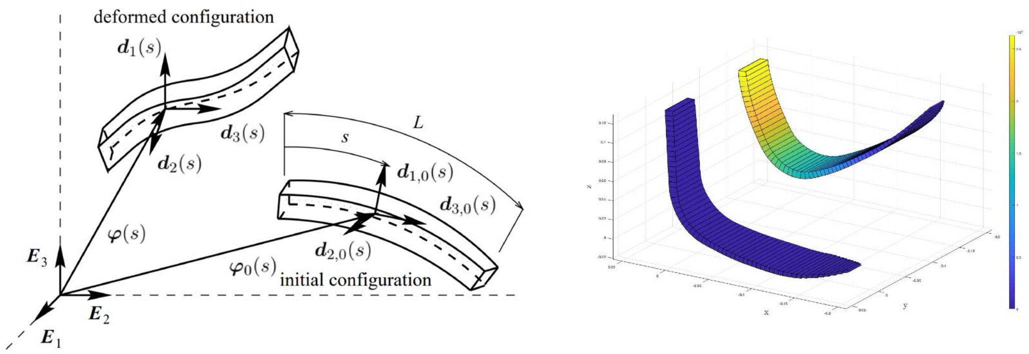

Figure 1: Visualisation of the initial and deformed configuration of a geometrically exact beam (left, based on [2]) and the resulting predeformed prosthesis model in Matlab (right).

The geometrically exact beam model allows for better representation of internal deformation energy during the simulation as well as reducing the computational effort, compared to standard finite element models. To check the model's implementation for consistency, a mesh study is performed. To this end, the number of nodes in the prosthesis model is increased after each simulation, resulting in an increasingly finer mesh, while keeping all other parameters and settings constant. The larger the number of nodes, the higher the resulting accuracy of the simulation. However, the computational cost grows as well. The finest mesh is used as a reference solution. The internal deformation energy is compared, while the prosthesis deforms under a magnified gravitational force.

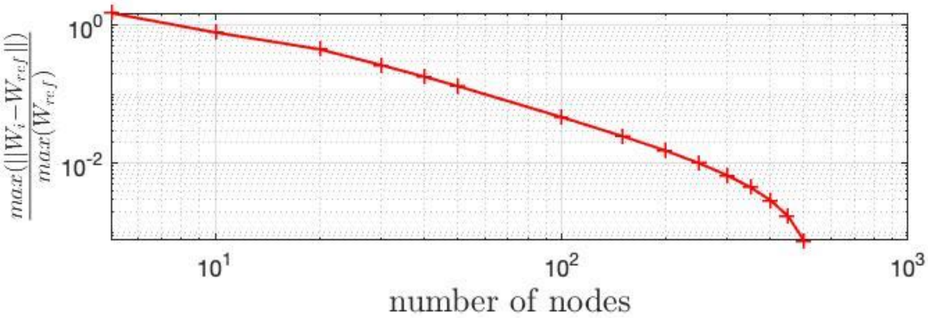

Figure 2: Visualisation of the internal deformation energy error when varying the number of nodes in the model.

In Figure 2, the solution converges up to very high numbers of nodes, where numerical artifacts can overlay the actual solution. This shows that the simulation converges to a solution when increasing the number of nodes, validating the implementation of the model. Furthermore, this also gives an indication of how large the simulation's error is due to the discretisation of the prosthesis with a limited number of nodes.

With the successful implementation of a prosthesis model, the next step is the consideration of epistemic uncertainty and to investigate its influence on the prediction of the walking comfort of the patient.

Acknowledgments This work is funded by the German Research Foundation (DFG) through the Priority Programme 'Polymorphic uncertainty modelling for the numerical design of structures– SPP 1886'.

References

[1] S. S. Antman, *Nonlinear Problems of Elasticity.* Springer, 1995.

[2] M. A. Crisfield and G. Jelenic. *Objectivity of strain measures in the geometrically exact three-dimensional beam theory and its finite-element implementation*, Proceedings of the Royal Society of London. Series A: Mathematical, Physical and Engineering Sciences, 455(1983):1125-1147, 1999.

[3] E. S. Scheiterer, *Simulation of a prosthetic foot modelled by a predeformed geometrically exact beam*, Master's Thesis, 2019

[4] M. Söhnlein, *Qualifzierung von Simulationsparametern einer Fussprothese durch numerische und experimentelle Modalanalyse*, Master's Thesis, 2019

4 Activities

4.1 Motion capture laboratory

Our motion analysis lab is equipped with a camera and marker based optical tracking system. This includes 10 Qualisys MoCap high speed cameras and 2 Qualisys high speed video cameras, Noraxon MyoMotion inertial sensors , Cyberglove III to measure hand joint angle kinematics, force plates, and Noraxon Desktop DTS electromyography sensors.

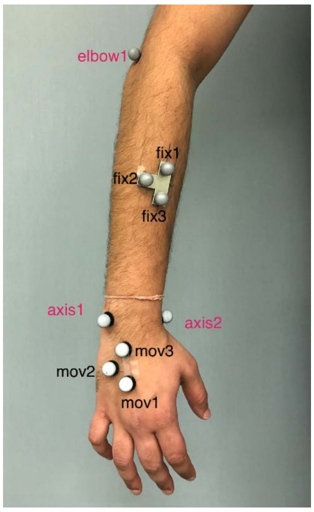

To perform motion capturing for small human actions, such as motion of hand digits, a frame was constructed to bring the cameras closer to the markers. With this setup, kinematic parameter identification for joints in the human hand, especially the wrist, the metacarpophalangeal and interpalangeal joints has been performed. This is an essential first step towards formulating a procedure for effective parameter identification to setup subject-specific models. This will enable us to perform biomechanical optimal control simulations with higher levels of confidence and use the results as measures of human performance.

4.2 Dynamic laboratory

The dynamic laboratory – modeling, simulation and experiment (Praktikum Technische Dynamik) adresses all students of the Technical Faculty of the Friedrich-Alexander-Universität Erlangen-Nürnberg. The aim of the practical course is to develop mathematical models of fundamental dynamical systems to simulate them numerically and compare the results to measurements from the real mechanical system. Here, the students learn both the enormous possibilities of computer based modeling and its limitations. The course contains one central programming exercise and six experiments observing various physical phenomena along with corresponding numerical simulations:

- programming training
- beating pendulums
- gyroscope
- ball balancer
- robot arm
- inverse pendulum
- balancing robot

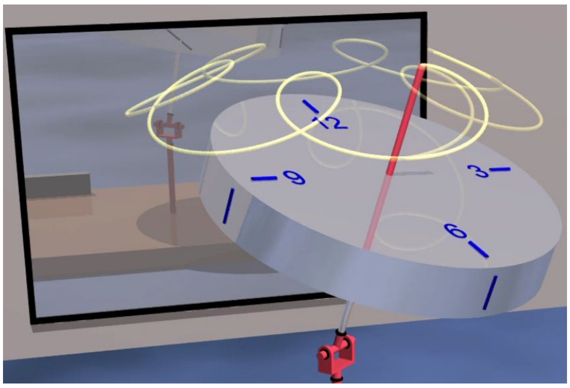

programming training

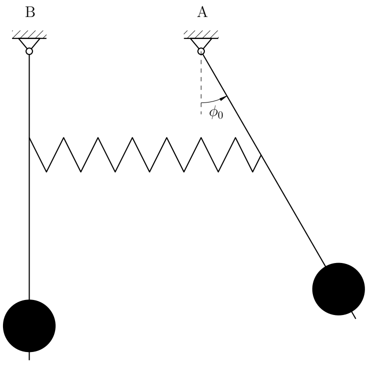

beating pendulums

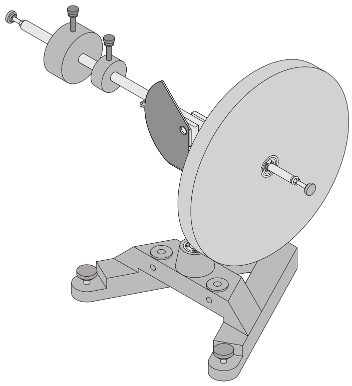

gyroscope

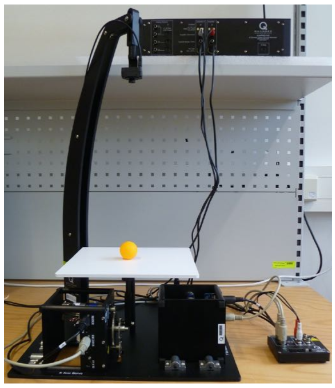

ball balancer

robot arm

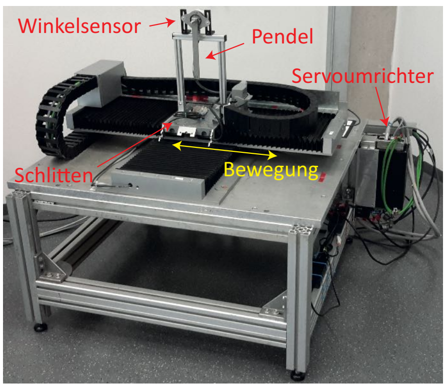

inverse pendulum

balancing robot

4.3 MATLAB laboratory

The MATLAB laboratory (Praktikum MATLAB) is offered to all students of the Technical Faculty of the Friedrich-Alexander-Universität Erlangen-Nürnberg. The course aims to teach the participants the basic skills of mathematical programming in MATLAB. The course is offered in conjunction with the Chair of Applied Mechanics (LTM), the Chair of Production Metrology (FMT) and the Chair of Engineering Design (KTmfk). The first lecture is an introductory programming session for MATLAB fundamentals. Thereafter, every chair presents a task related to mechanics and engineering, for example, the LTD task is to understand and simulate, the dynamics of a crane. The task is introduced to the students through a theory lecture, which is then followed by programming sessions.

4.4 Teaching

Winter semester 2019/2020

Dynamik starrer Körper (MB, ME, WING, IP, BPT, CE, MT)
Vorlesung — S. Leyendecker
Übung + Tutorium — D.Martonová, D. Holz
U. Phutane, M. Klebl
R. Sato Martín de Almagro

Mehrkörperdynamik (MB, ME, WING, TM, BPT, MT)
Vorlesung — S. Leyendecker
Übung — J. Penner

Biomechanik der Bewegung (MT)
Vorlesung + Übung — H. Lang

Numerische Methoden in der Mechanik (MT, MB, ME, WING, TM, BPT)
Vorlesung + Übung — H. Lang

Praktikum Technische Dynamik – Modellierung, Simulation und Experiment (MB, ME, WING)
S. Leyendecker
E.S. Scheiterer, D. Holz
J. Penner, U. Phutane
D. Phansalkar, M. Klebl
R. Sato Martín de Almagro

Praktikum Matlab (MB)
S. Leyendecker, U. Phutane

Summer semester 2019

Biomechanik (MT)
Vorlesung + Übung — S. Budday
geprüft 30 + 15 (WS 2018/2019)

Geometrische numerische Integration (MB, ME, WING, BPT)
Vorlesung — S. Leyendecker
Übung — E.S. Scheiterer
geprüft 4 + 0 (WS 2018/2019)

Statik und Festigkeitslehre (BPT, CE, ME, MWT, MT)		
Vorlesung		S. Leyendecker
Tutorium		U. Phutane, D. Holz D. Martonová, M. Klebl
Übung		D. Holz, U. Phutane J. Penner
geprüft	482 + 0 (WS 2018/2019)	

Praktikum Matlab (MB)		
Teilnehmer	34	S. Leyendecker, U. Phutane

Winter semester 2018/2019

Dynamik starrer Körper (MB, ME, WING, IP, BPT, CE, MT)		
Vorlesung		S. Leyendecker
Tutorium		U. Phutane, J. Penner D. Budday, D.Holz T. Wenger
Übung		J. Penner, D. Budday D. Holz
geprüft	388 + 141 (SS 2019)	

Mehrkörperdynamik (MB, ME, WING, TM, BPT, MT)		
Vorlesung		S. Leyendecker
Übung		T. Wenger
geprüft	65 + 14 (SS 2019)	

Praktikum Technische Dynamik – Modellierung, Simulation und Experiment (MB, ME, WING		
Teilnehmer	8	S. Leyendecker D. Holz, D. Budday T. Wenger, U. Phutane

Praktikum Matlab (MB)		
Teilnehmer	67	S. Leyendecker, U. Phutane

Additional exams

Hochschulpraktikum (M. Sc. Medizintechnik)		
geprüft	2	

4.5 Theses

Master theses

- Thomas Hufnagel
  Modelling a surface-based fluid cavity of a rat left ventricle using finite element method
- Myoungsic Kim
  Modelling and computing the nonlinear transmural fibre distribution of a rat heart using finite elements
- Eduard Sebastian Scheiterer
  Simulation of a prosthetic foot modelled by a predeformed geometrically exact beam
- Matthias Söhnlein
  Qualifizierung von Simulationsparameterneiner Fußprothese durch numerische und experimentelle Modalanalyse
- Linghui Wang
  Force distribution in the metacarpal head during activities of daily life
- Tianhui Zhang
  Determination of kinematic parameters through motion capturing of human hand
- Anja Boebel
  Kinematic reduction techniques in human hand modeling and its influence on grasping – Kinematically reduced Hand Models for grasping
- Emely Schaller
  Modelling the human heart – Comparison of MRI and simulation based cardiac motion
- Markus Lohmayer
  Towards a port-Hamiltonian approach to study Stirling-cycle devices
- Dhananjay Phansalkar
  Phase field fracture model – Investigation of the transition zone parameter

Project theses

- Jiafeng Wei
  Model-based control for a ball-balancer system

4.6 Seminar for mechanics

together with the Chair of Applied Mechanics LTM

06.03.2019 Dr. Rodrigo Takuro Sato Martín de Almagro
ICMAT, Madrid, Spain
A variational derivation of forced Euler-Lagrange and Euler-Poincaré equation and applications to error analysis

23.04.2019 Daniel Maier

Lehrstuhl für Umformtechnik und Gießereiwesen, TU München, Germany
Datengestützte Kompensation von massivumgeformten Bauteilen mittels materieller Punktverfolgung

28.06.2019 Prof. Dr.-Ing. habil. Ellen Kuhl
Mechanical Engineering, Living Matter Lab, Stanford University, USA
Machine learning in drug development

03.07.2019 Prof. Jochen Guck
Max-Planck-Institut für die Physik des Lichts, Erlangen, Germany
Soft Matters – Mechanosensing of neural cells in the CNS

16.09.2019 Dengpeng Huang
Institute of Continuum Mechanics, Leibniz Universität Hannover,Germany
Data-driven computational modelling of metal machining processes using machine learning and OTM method

16.09.2019 Dr.-Ing. Armin Widhammer
OBH SYSTEM AG, Weßling, Germany
Variation of Reference Strategy – Generation of Optimized Cutting Patterns for Textile Fabrics

17.09.2019 Michael Jäger
Friedrich-Alexander-Universität Erlangen-Nürnberg
Modal Derivatives based Reduction Method for nonlinear Finite Elements using Shape Adaption.

17.09.2019 Ahmet Ismail
Technische Hochschule Lübeck, Germany
Kinematische Analyse von Protein-Konformationen mit Hilfe des Rouché-Cpaelli-Theorem

17.09.2019 M.Sc. Yu Zou
Friedrich-Alexander-Universität Erlangen-Nürnberg
Computer-aided Mechanical Engineering

30.10.2019 Prof. Anja Boßerhoff
Lehrstuhl für Biochemie und Molekulare Medizin, Friedrich-Alexander-Universität Erlangen-Nürnberg
Impact of the microenvironment on melanoma development and progression

20.11.2019 Dr. Andrea Thorn
Rudolf Virchow Center for Experimental Biomedicine, Würzburg, Germany
The role of models in the structure determination of biological macromolecules

12.12.2019 Dr. Thomas Boudou
Laboratoire Interdisciplinaire de Physique, Université Grenoble Alpes
Engineering 3D microtissues

4.7 Editorial activities

Advisory and editorial board memberships Since January 2014, Prof. Dr.-Ing. habil. Sigrid Leyendecker is a member of the advisory board of the scientific journal Multibody System Dynamics, Springer. She is a member of the Editorial Board of ZAMM – Journal of Applied Mathematics and Mechanics / Zeitschrift für Angewandte Mathematik und Mechanik since January 2016 and since 2017 runs a second term as member of the managing board of the International Association of Applied Mathematics and Mechanics (GAMM), as well as a member of the executive council of the German Association for Computational Mechanics (GACM) and member of the General Council of the International Association for Computational Mechanics (IACM).

Since October 2017, Prof. Dr.-Ing. habil. Sigrid Leyendecker is an elected member of the Faculty Council of the Faculty of Engineering at the Friedrich-Alexander-Universität Erlangen-Nürnberg, and in April 2019 was elected deputy Chair of the Qualification Assessment Committee (Eignungsfeststellungsverfahrens-(EFV-)Kommission) of the Bachelor's degree programme Medical Engineering, at the Friedrich-Alexander-Universität Erlangen-Nürnberg.

4.8 Long Night of Sciences at the Friedrich-Alexander-Universität Erlangen-Nürnberg (Die Lange Nacht der Wissenschaften)

On October 19t, 2019, the Friedrich-Alexander-Universität Erlangen-Nürnberg organised the Long Night of Sciences, an event where families, students, politicians and scientist are welcome to visit more than 100 events in which technology, medicine, natural and engineering sciences as well as humanities, economics and social sciences are represented. The Chair of Applied Dynamics participated and showed interesting experiments in its laboratories, such as:

- Carrera race – a playful experiment for optimal control
- Angular momentum conservation and Lagrange gyro
- Balancing Lego robot on two wheels
- Inverse pendulum – human against machine
- Beating phenomenon – example of two floating pendulums

Some experiment were well suited and popular for children such as to try to "invert" a pendulum simply by controlling it with a joystick without the help of numerical control algorithms. The Chair received the visit of the Minister of the Interior, Joachim Herrmann, who was encouraged to try the Carrera race experiment. The ambiance was blissful and with an exeptionally positive feedback.



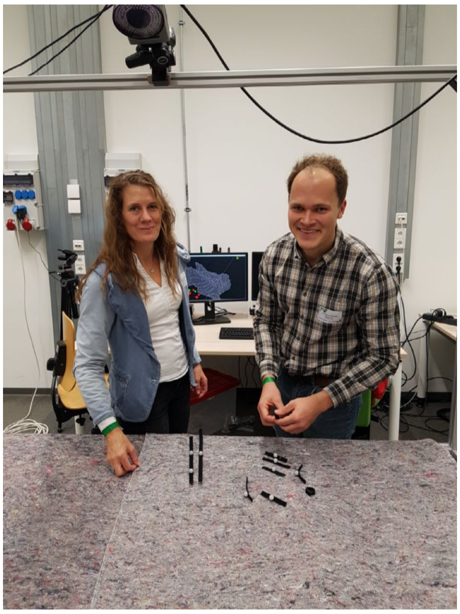


5 Publications

5.1 Reviewed journal publications

1. R. Hoffmann, B. Taetz, M. Miezal, G. Bleser and S. Leyendecker. “On optical data-guided optimal control simulations of human motion”. *Multibody System Dynamics*, pp. 1-22, 2019.

2. M.T. Duong, D. Holz, M. Alkassar, S. Dittrich and S. Leyendecker. “Interaction of the mechano-electrical feedback with passive mechanical models on a 3D rat left ventricle: a computational study”. *Frontiers in Physiology, section Computational Physiology and Medicine*, Vol. 10, pp. 1041, DOI 10.3389/fphys.2019.01041, 2019.

3. D. Pivovarov, V. Hahn, P. Steinmann, K. Willner and S. Leyendecker. “Fuzzy dynamics of multibody systems with polymorphic uncertainty in the material microstructure”. *Computational Mechanics*, Vol. 64, pp. 1601-1619, DOI 10.1007/s00466-019-01737-9, 2019.

4. D. Pivovarov, K. Willner, P. Steinmann, S. Brumme, M. Müller, T. Srisupattarawanit, G.P. Ostermeyer, C. Henning, T. Ricken, S. Kastian, S. Reese, D. Moser, L. Grasedyck, J. Biehler, M. Pfaller, W. Wall, T. Kohlsche, O. von Estorff, R. Gruhlke, M. Eigel, M. Ehre, I. Papaioannou, D. Straub and S. Leyendecker. “Challenges of order reduction techniques for problems involving polymorphic uncertainty”. *GAMM-Mitteilungen*, e201900010, DOI 10.1002/gamm.201900011, 2019.

5. M. Eisentraudt and S. Leyendecker. “Fuzzy uncertainty in forward dynamics simulation”. *Mechanical Systems and Signal Processing*, Vol. 126, pp. 590-608, DOI 10.1016/j.ymssp.2019.02.036, 2019.

5.2 Invited lectures

1. S. Leyendecker. *Musculoskeletal digital human models in assembly planning*, Challenge Workshop – Mathematical Modeling of Biomedical Problems, Erlangen, Germany, 12-13 December 2019.

2. S. Leyendecker. *Mixed order and multirate variational integrators for the simulation of dynamics on diferent time scales.* Instituto de ciencias matemáticas, Madrid, Spain, 22 October 2019.

3. S. Leyendecker. *Mixed order and multirate variational integrators for the simulation of dynamics on diferent time scales.* Isaac Newton Institute for Mathematical Sciences, Cambridge, UK, September 2019.

5.3 Conferences and proceedings

1. S. Leyendecker. “Geometric numerical integration in simulation and optimal control”. *International Congress on Industrial and Applied Mathematics (ICIAM)*, Valencia, Spain, 15-19 July 2019.

2. D. Budday, S. Leyendecker and H. van den Bedem, “Kino-Geometric Modeling: Insights into Protein Molecular Mechanisms”, *Proc. Appl. Math. Mech.*, *PAMM*, Vol. 19, DOI:10.1002/pamm.201900448, 2019.

3. J. Penner and S. Leyendecker, “A Hill Muscle Actuated Arm Model with Dynamic Muscle Paths”, In: *Proceedings of the IFToMM World Congress on Mechanism and Machine Science and 9th ECCOMAS Thematic Conference on Multibody Dynamics*, pp. 52-59, Krakow, Poland, 30 June - 4 July, 2019.

4. U. Phutane, M. Roller, S. Björkenstamand and S. Leyendecker. “Optimal Control Simulations of Two-Finger Precision Grasps”. In:*Proceedings of the IFToMM World Congress on Mechanism and Machine Science and 9th ECCOMAS Thematic Conference on Multibody Dynamics*, pp. 60-67, Krakow, Poland, 30 June - 4 July, 2019.

5. D. Holz, M.T. Duong, M. Alkassar, S. Dittrich and S. Leyendecker, “Computational study of ventricular fibrillation by considering a strongly coupled electromechanical rat heart model”, *Proc. Appl. Math. Mech.*, *PAMM*, Vol. 19, DOI 10.1002/pamm.201900227, Vienna, Austria 18-22 February, 2019.

6. U. Phutane, M. Roller and S. Leyendecker, “On grasp based objectives in human grasping simulation”, *Proc. Appl. Math. Mech.*, *PAMM*, Vol. 19, DOI 110.1002/pamm.201900226, Vienna, Austria, 18-22 February, 2019.

7. J. Penner and S. Leyendecker, “Biomechanical simulations with dynamic muscle paths on NURBS surfaces”, *Proc. Appl. Math. Mech.*, *PAMM*, Vol. 19, DOI 10.1002/pamm.201900230, Vienna, Austria, 18-22 February, 2019.

6 Social events

Visit of the Wildpark Hundshaupten 12.03.2019




Visit of Berg in Erlangen 11.06.2019


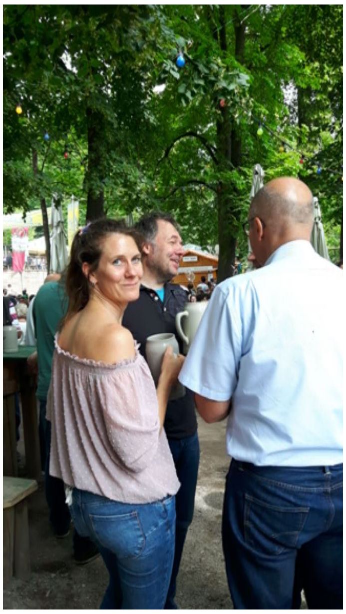

Student summer grill 25.07.2019

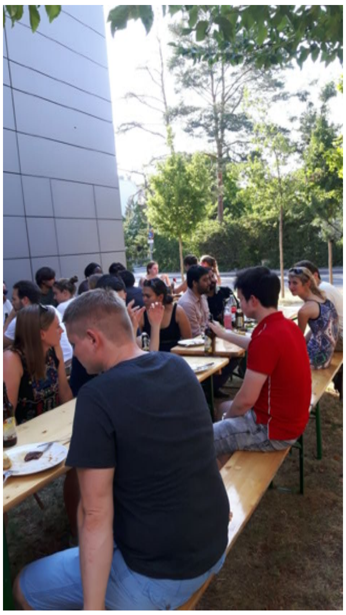

Visit to the climbing park 27.08.2019

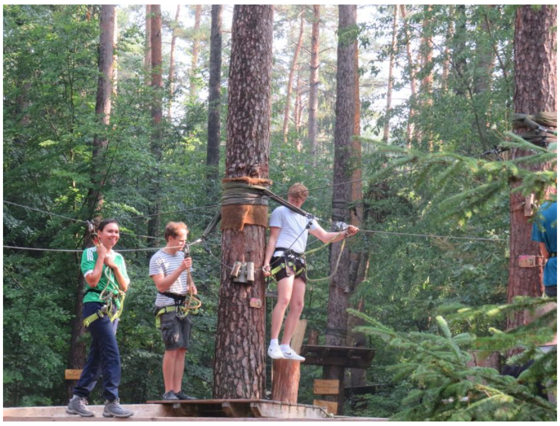

Christmas party together with LTM 04.12.2019

Farewell and onboarding lunch of team members